Physics – Uspekhi **46** (11) 1121 – 1136 (2003)

REVIEWS OF TOPICAL PROBLEMS PACS numbers: 11.55.Jy, **12.38. – t**, 12.40.Na

Pomeranchuk singularity and high-energy hadronic interactions

A B Kaĭdalov

DOI: 10.1070/PU2003v046n11ABEH001640

Contents

Abstract. The Reggeon approach to high-energy hadronic interactions is reviewed and the dynamics of Regge poles in QCD is discussed with emphasis on the Pomeranchuk singularity in the complex angular momentum plane (pomeron). A possible link between the pomeron trajectory and the spectrum of glueballs is considered. High-energy hadronic interactions are described with the framework based on the Reggeon theory. It is shown that the concept of a pomeron is important not only for the theory of hadronic interactions but also for understanding high-energy heavy ion collisions and the small-x physics of deep inelastic scattering.

1. Introduction

Investigation of high-energy hadronic interactions is firmly connected with the name of I Ya Pomeranchuk. He was one of the founders of many important aspects of the modern theory of strong interactions at high energies. Among them is the formulation of the theory of diffraction dissociation of hadrons, done together with E L Feinberg [1]. At present, this is a broad field of both theoretical and experimental studies. The first asymptotic theorem on the equality of total interaction cross sections for particles and antiparticles was formulated by Pomeranchuk [2] and is known as the Pomeranchuk theorem. In the Reggeon theory, which is the main subject of this review, Pomeranchuk has obtained many important results [3], and the leading Regge pole, which determines high-energy behavior of diffractive processes, has been called [4] the Pomeranchuk pole, or pomeron. This pole has vacuum quantum numbers and plays a fundamental role in the theory of high-energy interactions.

With the advent of QCD as the microscopic theory of strong interactions, investigation of the dynamics of Regge poles and of the pomeron in particular reached a new level. The asymptotic freedom of QCD allows applying the perturbation theory to processes with large momentum transfer. On the other hand, large-distance phenomena, where the coupling constant is not small and nonperturbative effects are important, still present a problem for the theory. It is very important to understand QCD in this large-distance domain. Processes with small momentum transfer, which give the dominant contribution to high-energy hadronic interactions and are related to the dynamics of the pomeron, provide a natural testing ground for theoretical ideas and QCD-based models of large-distance dynamics. In Section 2, we discuss both perturbative and nonperturbative aspects of the pomeron in QCD.

In Section 3, the approach to high-energy hadronic interactions based on the Reggeon calculus and the $1/N$-expansion in QCD [5 – 8] is presented. Extra dynamical input is provided by the color-tube, or string models [9 – 13], which are closely related to the space-time picture of interaction in the $1/N$-expansion. The existence of string-like configurations of gluonic fields is confirmed by lattice calculations in QCD.

The powerful method of the Reggeon theory, based on analyticity and unitarity, has been developed for describing soft hadronic interactions at high energies. In this review, we show how to incorporate the QCD-based models into this general scheme. As a result, many relations between parameters of the Reggeon theory are established. The quark – gluon strings model (QGSM) [14, 15] and the dual parton model [16, 17] based on these ideas are discussed in more detail and are compared with experimental data on multiparticle production in hadronic collisions.

A B Kaĭdalov Institute for Theoretical and Experimental Physics
B. Cheremushkinskaya ul. 25, 119259 Moscow, Russian Federation
Tel. (7-095) 129 94 31
E-mail: kaidalov@heron.itep.ru

Received 30 April 2003, revised 21 June 2003
Uspekhi Fizicheskikh Nauk **173** (11) 1153 – 1170 (2003)
Translated by A B Kaĭdalov; edited by A M Semikhatov

Section 4 is devoted to the modern status of the Pomeranchuk theorem and the problem of the 'odderon' (singularity with negative C-parity and signature, which can lead to a difference between scattering of particles and antiparticles) in QCD.

In Section 5, we apply the formalism to interactions of virtual photons with nucleons and nuclei. A qualitative picture of diffractive dissociation of a virtual photon is described and a model based on this picture and methods of the Reggeon theory is formulated. This model gives a unified description of both structure functions of the proton in a broad range of virtualities Q^2 and diffractive dissociation of a virtual photon in this range. The model leads to definite predictions for shadowing of nuclear structure functions.

The last section is devoted to heavy ion collisions. We emphasize the importance of shadowing effects in heavy ion collisions. It is shown how these effects modify predictions of the Glauber model for inclusive spectra and particle densities at very high energies. Comparison with RHIC results is made.

2. Theory of Reggeons

2.1 The Reggeon concept

The complex angular momentum method was first introduced by Regge in nonrelativistic quantum mechanics [18]. In relativistic theory, it connects the high-energy behavior of scattering amplitudes with the singularities in the complex angular momentum plane of the partial wave amplitudes in the crossed channel [19, 20]. The simplest singularities are poles (Regge poles). A Regge-pole exchange is a natural generalization of the usual exchange of a particle with spin J to complex values of J. This method establishes an important connection between high-energy scattering and the spectrum of hadrons.

We consider a reaction $1+2\to 3+4$ at high energies $s=(p_1+p_2)^2\gg m^2$ and fixed momentum transfer $t=(p_1-p_3)^2\sim m^2$. An exchange by a particle of spin J in the t-channel (Fig. 1a) leads to the amplitude

$$T(s,t)=g_1g_2\left(\frac{s}{s_0}\right)^J(M_J^2-t)^{-1}\,, \tag{1}$$

where $s_0=1$ GeV^2, g_i are the coupling constants, and M_J is the mass of the exchanged particle.

It follows from Eqn (1) that for particles with spins $J\geqslant 2$, the amplitude grows faster than s^1, thus violating the Froissart bound [21]. According to the statement of the Froissart bound, which follows from general properties of relativistic quantum theory, amplitudes of binary reactions in the physical region cannot grow faster than $s\ln^2(s)$ as $s\to\infty$. On the other hand, we know from experiment that there are many hadron resonances with spins $J\geqslant 2$. This problem can be solved by the introduction of Regge poles. It should be taken into account that expression (1) for the amplitude is valid, strictly speaking, only close to the pole position $t\approx M_J^2$ and can be strongly modified away from the pole. The Regge pole model gives an exact form of this modification and takes account of exchanges by states of different spins (Fig. 1b). The corresponding amplitude has the form

$$T(s,t)=f_1(t)f_2(t)\left(\frac{s}{s_0}\right)^{\alpha(t)}\eta\big(\alpha(t)\big)\,, \tag{2}$$

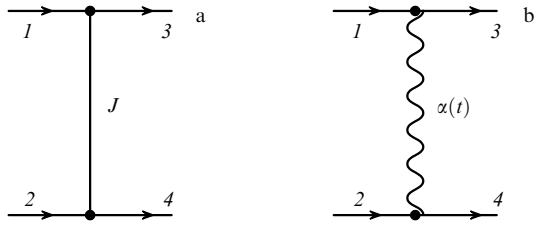

Figure 1. (a) Diagram for exchange by a particle with spin J in the t-channel. (b) Diagram for exchange by a Regge pole.

where $\alpha(t)$ is the Regge trajectory, which is equal to spin J of the corresponding particle at $t=M_J^2$. The function $\eta(\alpha(t))=-(1+\sigma\exp(-\mathrm{i}\pi\alpha(t))$ is a signature factor and $\sigma=\pm 1$ is a signature. It appears because in relativistic theory, the analytic continuation of partial wave amplitudes to complex values of angular momenta J must be considered separately for even ($\sigma=+1$) and odd ($\sigma=-1$) values of J. It should be emphasized that a single Regge exchange corresponds to an exchange of particles or resonances that are 'situated' on the trajectory $\alpha(t)$. For example, if $\alpha(t)=J$, where J is an even (odd) integer for $\sigma=+1(-1)$ at $t=M_J^2$ and M_J^2 is less than the threshold for transition to several hadrons ($4m_\pi^2$ for particles that can decay into two pions), then the Regge amplitude transforms into particle exchange amplitude (2) with

$$g_1g_2=\frac{f_1(M_J^2)f_2(M_J^2)2}{\pi\alpha'(M_J^2)}\,.$$

If M_J is larger than the particle creation threshold, then $\alpha(t)$ is a complex function and can be written for $t\approx M_J^2$ in the form

$$\alpha(t)=J+\alpha'(M_J^2)(t-M_J^2)+\mathrm{i}\,\mathrm{Im}\,\alpha(M_J^2)\,. \tag{3}$$

In this case, for $\mathrm{Im}\,\alpha(M_J^2)\ll 1$, Regge pole amplitude (2) corresponds to an exchange in the t-channel by a resonance and has the Breit – Wigner form

$$T(s,t)=-g_1g_2\left(\frac{s}{s_0}\right)^J(t-M_J^2+\mathrm{i}M_J\Gamma_J)^{-1} \tag{4}$$

with the width $\Gamma_J=\mathrm{Im}\,\alpha(M_J^2)/\big(M_J\,\alpha'(M_J^2)\big)$.

Thus, the reggeization of particle exchanges leads to a natural resolution of the above problem concerning violation of the Froissart bound: Regge trajectories that correspond to higher-spin particles can have $\alpha(t)\leqslant 1$ in the physical region of high-energy scattering $t\leqslant 0$ and the corresponding amplitudes grow with s not faster than s^1, satisfying the Froissart bound. We see later in this section that the experimental information on spectra of hadrons and high-energy scattering processes nicely confirms this theoretical expectation. The only exception is the Pomeranchuk pole, which determines high-energy behavior of diffractive processes. We pay special attention to the properties of the pomeron below.

Representation for the scattering amplitude as a sum of contributions of singularities in the complex angular momentum plane can be obtained from general properties of the relativistic S-matrix theory: analyticity, unitarity, and crossing. The two-particle unitarity condition in the t-channel

analytically continued to complex values of angular momentum allows proving that the Regge poles have definite conserved quantum numbers: signature, parity, baryon quantum number, isospin, etc.

Information on trajectories of Regge poles can be obtained for $t \leqslant 0$ from data on two-body reactions at large s and for $t > 0$ from our knowledge of the hadronic spectrum.

There can be many trajectories with the same quantum numbers indicated above, which differ by a quantum number analogous to the radial quantum number. Such trajectories are usually called 'daughter' trajectories; the masses of the corresponding resonances (with the same value of J) for them are higher than those for the leading trajectory.

Trajectories for some well-established bosonic Regge poles are shown in Fig. 2. Note that all these trajectories have $\alpha_i(t) \leqslant 0.5$ for $t \leqslant 0$. One of the most interesting properties of these trajectories is their surprising linearity. This is usually interpreted as a manifestation of strong forces between quarks at large distances, which lead to color confinement. The linearity of Regge trajectories indicates a string picture of the large-distance dynamics between quarks, and it was a basis of dual and string models of hadronic interactions.

Other properties of mesonic Regge trajectories, which are evident from Fig. 2, are the exchange and isospin degeneracies: trajectories with different signatures and $I = 0$ or $I = 1$ (but with the same σP) are degenerate with good accuracy (at least in the region $t > 0$). This is also in agreement with dual models or approaches based on the $1/N$-expansion in QCD. In dual or string models of hadrons, the daughter trajectories must be parallel to the leading one and must be displaced by integers in the j-plane. Experimental information on the daughter trajectories is rather limited but it does not contradict these predictions.

Information on mesonic Regge trajectories in the region of negative t, obtained from the analysis of binary reactions at high energies, fits quite well the lines shown in Fig. 2 obtained from the spectrum of resonances. The most detailed information exists for the ρ- and A_2-trajectories, which contribute to the respective reactions $\pi^- p \to \pi^0 n$ and $\pi^- p \to \eta n$.

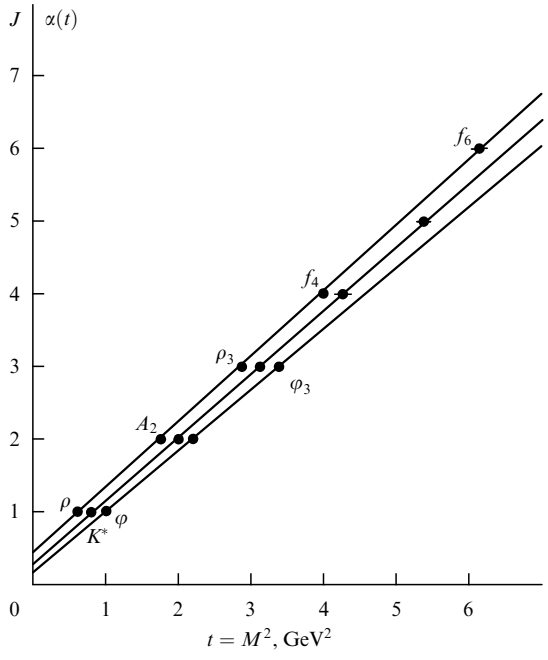

Figure 2. Trajectories of some bosonic Regge-poles.

Experimental data on the spectrum of baryons show that baryonic trajectories, as well as mesonic ones, are nearly straight lines in the variable t with the universal slope $\alpha' \approx 1$ GeV^{-2}. This universality of the slopes is natural in the string picture of baryons with a quark and a diquark at the ends.

We now discuss the properties of the pole that has a special status in the Regge approach to particle physics — the Pomeranchuk pole, or the pomeron. This pole was introduced into the theory in order to account for the behavior of total interaction cross sections and elastic scattering at high energies. In the Regge pole model, the amplitude of high-energy elastic scattering has the form of Eqn (2) and the total interaction cross section, which by the optical theorem is connected to Im $T(s, 0)$ (in our normalization, it has the form $\sigma^{\text{tot}}(s) = \text{Im}\, T(s, 0)/s$ for $s \gg m^2$), can be written as a sum of the Regge pole contributions,

$$\sigma^{\text{tot}}(s) = \sum_k b_k(0)(s)^{\alpha_k(0)-1}. \tag{5}$$

The poles shown in Fig. 2 have $\alpha_k(0) < 1$ and therefore their contributions to $\sigma^{\text{tot}}(s)$ decrease as $s \to \infty$. However, experimental data show that the total cross sections of hadronic interactions have a weak energy dependence at $s \sim 100$ GeV^2 and slowly increase with energy at higher energies. In the Regge pole model, this can be related to the pole with the intercept $\alpha_P(0) \approx 1$. This pole is usually called the pomeron, or the vacuum pole, because it has the quantum numbers of the vacuum: positive signature, parity, G (or C) parity, and isospin $I = 0$.

It is usually assumed in QCD that this pole is related to gluonic exchanges in the t-channel. The resonances on its trajectory in the region of positive t are therefore associated with glueballs (bound states of gluons). We discuss the possible relation between QCD and Regge theory in more detail below.

The value of the intercept of the pomeron plays an important role in the Regge theory. If $\alpha_P(0) = 1$, as was assumed initially, all the total interaction cross sections tend to a constant at very high energies. This theory, however, has some intrinsic difficulties and must satisfy many constraints in order to be consistent with unitarity. Besides, experimental data indicate that $\sigma_{hN}^{(\text{tot})}$ grow with energy. This logarithmic growth of total cross sections at very high energies is in accord with the $\ln^2(s/s_0)$ behavior that follows from the Froissart theorem [21]. Thus, the supercritical pomeron theory with $\alpha_P(0) > 1$ is widely used at present. In a model with only Regge poles taken into account, the assumption $\alpha_P(0) > 1$ would lead to a power-like growth of total cross sections, thus violating the Froissart bound. In this case, however, other singularities in the j-plane — moving branch points [22, 23] — should be taken into account and their contributions allow one to restore unitarity and to obtain the high-energy behavior of scattering amplitudes that satisfies the Froissart bound. Properties of these moving cuts are considered below.

In accordance with the unitarity, imaginary parts of the Regge pole exchange amplitudes in binary reactions are related to certain intermediate states in the s-channel. At high energies, these are many-body states, described by the multiperipheral model of particle production [24]. In this model, the number of produced particles increases logarith-

mically with energy and the particles produced have limited transverse momenta and a flat distribution in rapidity. In this model, it is possible to obtain the leading Regge pole (pomeron) with an intercept close to unity [25]. The multiparticle content of the pomeron in the QCD-based models are discussed below.

2.2 Regge poles in QCD

The remarkable linearity of trajectories for Regge poles corresponding to the known $q\bar{q}$-states indicates essentially nonperturbative, string-like dynamics of these objects in QCD. A nonperturbative method that can be used in QCD for describing large-distance dynamics is the $1/N$-expansion (or topological expansion) [5–7].

In this approach, the quantities $1/N_c$ [5] and $1/N_{lf}$ [6] (where N_c is the number of colors and N_{lf} is the number of light flavors) are considered small parameters and the amplitudes and the Green functions are expanded in terms of these quantities. In QCD, $N_c = 3$ and $N_{lf} \approx 3$, and the expansion parameter does not look small enough. But we see below that in most cases, the expansion parameter is $1/N_c^2 \sim 0.1$.

In the formal limit $N_c \to \infty$ ($N_{lf}/N_c \to 0$), QCD has many interesting properties and has been intensively studied theoretically. There is hope to obtain an exact solution of the theory in this limit (the 2-dimensional QCD has been solved in the limit $N_c \to \infty$). However, this approximation is rather far from reality because resonances are infinitely narrow ($\Gamma \sim 1/N_c$) in this limit. The case where the ratio $N_{lf}/N_c \sim 1$ is fixed and the expansion in $1/N_{lf}$ (or $1/N_c$) is carried out [6] seems more realistic.

This approach is sometimes called the topological expansion because a given term of this expansion corresponds to an infinite set of Feynman diagrams with definite topology.

The first term of the expansion corresponds to planar diagrams of the type shown in Fig. 3 for the binary reaction. These diagrams always have the valence quarks of the colliding hadrons as their border lines. At high energies, they should correspond to exchanges by secondary Regge poles $\alpha_R(\rho, A_2, \omega, ...)$ 'made of' light quarks. The s-channel cut of the planar diagram in Fig. 3a is shown in Fig. 3b. Here and in what follows, we do not show the internal lines of gluons and quark loops.

We note that the planar diagrams correspond to annihilation of a valence quark and an antiquark belonging to the colliding hadrons.

The topological classification of diagrams in QCD leads to many relations between the parameters of the Reggeon theory, hadronic masses, widths of resonances, and total cross sections (see [15] for a review). All these relations are in good agreement with experiment.

The contribution of the planar diagrams to the total cross section decreases with energy as

$$\frac{1}{s^{(1-\alpha_R(0))}} \approx \frac{1}{\sqrt{s}}\,.$$

This decrease is related to the fact that quarks have spin $1/2$ and in the lowest order of perturbation theory, an exchange by two quarks in the t-channel leads to the behavior $\sigma \sim 1/s$, which corresponds to the intercept $\alpha_R(0) = 0$. The interaction between quarks should lead to an increase of the intercept to the observed value $\alpha_R(0) \approx 0.5$.

The calculation of Regge trajectories in QCD is a difficult problem, even for planar diagrams. It was considered in [26] using the Wilson-loop path integral method [27]. It was shown that under a reasonable assumption about large distance dynamics — the minimal-area law $\langle W \rangle \sim \exp(-\sigma S_{min})$ for a Wilson loop at large distances — it is possible to calculate the spectrum of $q\bar{q}$-states. The minimal-area law is equivalent to the quark confinement at large distances and is confirmed by numerous lattice calculations. The resulting spectrum for light quarks is described with good accuracy by a very simple formula

$$\frac{M^2}{2\pi\sigma} = L + 2n_r + c_1\,, \tag{6}$$

where L and n_r are the orbital and radial quantum numbers. This spectrum corresponds to an infinite set of linear Regge trajectories similar to the one of dual and string models.

In Ref. [26], spin effects have not been taken into account. Realistic calculations of masses of hadrons, which take spin effects, perturbative interactions at small distances, and quark loops into account, have recently been carried out [28]. The resulting Regge trajectories are in good agreement with the experimental ones shown in Fig. 2.

2.3 Glueballs and the pomeron in QCD

In the $1/N$-expansion of QCD, the pomeron corresponds to the class of cylinder-type diagrams shown in Fig. 4. Such diagrams for elastic scattering or reactions without a quantum number exchange in the t-channel are shown in Fig. 4a, where the valence quarks of colliding hadrons are conserved in the process of interaction. The s-channel cuttings of these diagrams correspond to the multiparticle production configurations shown in Fig. 4b. These configurations correspond to production of two chains of particles and each chain has the same structure as the one shown for the planar diagram in Fig. 3b. From the t-channel standpoint,

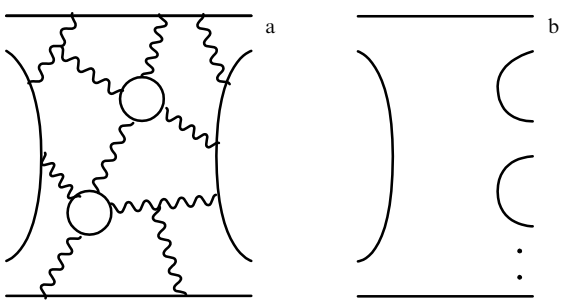

Figure 3. (a) Planar diagrams for reaction $ab \to cd$, (b) same for reaction $ab \to X$. Full lines denote quarks, wavy lines gluons.

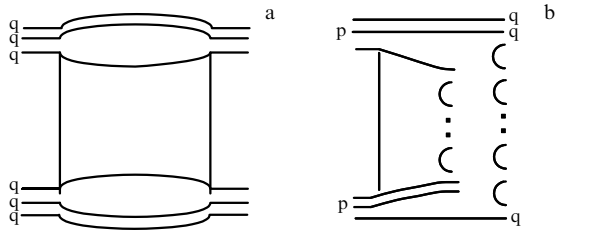

Figure 4. (a) Cylinder type diagrams and (b) cutting of these diagrams in the s-channel.

the cylinder diagrams are due to the exchange by gluons in the t-channel. From the topological classification standpoint, the cylinder diagrams correspond to a sphere with two boundaries, given by the valence quark lines of colliding hadrons.

It is very important to calculate the pomeron trajectory in QCD. Perturbative calculations of the pomeron in QCD were carried out by L Lipatov and collaborators [29] (BFKL pomeron) many years ago. The pomeron is related to a sum of ladder-type diagrams with exchange by reggeized gluons. Reggeization of gluons (as well as quarks) is an important property of QCD (at least in perturbation theory). In the leading approximation of the perturbation theory, the expression for the intercept of the pomeron is [29]

$$\Delta \equiv \alpha_{\mathrm{P}}(0) - 1 = \frac{4N_{\mathrm{c}} \ln 2}{\pi}\, \alpha_{\mathrm{s}}\,. \tag{7}$$

In this approximation, $\Delta \approx 0.5$. Order-α_{s} corrections to expression (7) calculated recently [30] strongly decrease the value of Δ. The value of Δ depends on the choice of the renormalization scheme and renormalization scale. The choice of the physical (BLM) scheme leads to stable results for Δ $\Delta \approx 0.17$, which is independent of the virtuality of the process [31].

The influence of the effects that are not described by the QCD perturbation theory on the pomeron trajectory and its relation to the spectrum of glueballs was considered in [32, 33] using the Wilson-loop path integral method discussed above in the case of $q\bar{q}$-Regge poles.

Glueballs are among the most intriguing objects in both experiment and theory. While the experimental situation is not yet settled, lattice simulations [34, 35] yield an overall consistent picture of the lowest ($M < 4$ GeV) mass spectrum of glueballs. The mass scale and level ordering of the glueball spectra differ from those of meson spectra, yielding unique information about the nonperturbative structure of the gluonic vacuum.

With the spin effects and quark loops neglected, the spectrum of two-gluon glueballs is determined by the large-distance expression for the Wilson loop given above, with the only difference that the string tension (σ_{fund}) for the $q\bar{q}$ system is changed to σ_{adj}.

The value of σ_{adj} can be found from the string tension σ_{fund} of the $q\bar{q}$ system by multiplying it with 9/4, as follows from the Casimir scaling observed on the lattices. Taking the experimental Regge slope for mesons $\alpha' = 0.89$ GeV^{-2}, we obtain $\sigma_{\mathrm{fund}} = 0.18$ GeV^2 and $\sigma_{\mathrm{adj}} \approx 0.40$ GeV^2.

The spin splittings for glueball masses were calculated in [33], assuming that spin effects can be treated as small perturbations. The largest correction is obtained for the lowest state from the spin–spin interaction. The calculated spectrum of glueballs [33] is in perfect agreement with the results of lattice calculations (Table 1).

The leading gluon Regge trajectory calculated within this approach is close to the $q\bar{q}$ Regge trajectories f and f' in the region of small t. In this region, the mixing between gluonic and $q\bar{q}$ Regge trajectories is therefore important. The mixing effects and accounting of small distances by the QCD perturbation theory allow one to obtain a phenomenologically acceptable intercept of the pomeron trajectory and lead to an interesting pattern of vacuum trajectories in the positive-t region [33].

It is important to understand which region of transverse momenta of produced particles makes the dominant contribution at high energies. In the case where large transverse momenta of the produced gluons are important and small-distance dynamics is the dominant mechanism, the pomeron is usually called 'hard'. Such a situation occurs for the leading-order BFKL pomeron. If, on the other hand, small momentum transfers are dominant, the pomeron is called 'soft'. We emphasize that in the approach discussed above, the 'hard' and 'soft' pomerons are mixed. The equation for the pomeron singularity contains both nonperturbative effects and perturbative dynamics. Therefore, the resulting 'physical' pole is a state due to both 'soft' and 'hard' interactions. Thus, the pomeron in QCD has a very rich and interesting structure.

Table 1. Comparison of predicted glueball masses with lattice data.

J^{PC}	M, GeV paper [33]	Lattice data		$M[G]/M[0^{-+}]$		Difference, %
		paper [34]	paper [35]	paper [33]	paper [34]	
0^{++}	1.58	1.73 ± 0.13	1.74 ± 0.05	0.62	0.67 (2)	−7
0^{++*}	2.71	2.67 ± 0.31	3.14 ± 0.10	1.06	1.03 (7)	3
2^{++}	2.59	2.40 ± 0.15	2.47 ± 0.08	1.01	0.92 (1)	9
2^{++*}	3.73	3.29 ± 0.16	3.21 ± 0.35			
0^{-+}	2.56	2.59 ± 0.17	2.37 ± 0.27			
0^{-+*}	3.77	3.64 ± 0.24		1.47	1.40 (2)	5
2^{-+}	3.03	3.1 ± 0.18	3.37 ± 0.31	1.18	1.20 (1)	−1
2^{-+*}	4.15	3.89 ± 0.23		1.62	1.50 (2)	8
3^{++}	3.58	3.69 ± 0.22	4.3 ± 0.34	1.40	1.42 (2)	−2
1^{--}	3.49	3.85 ± 0.24		1.36	1.49 (2)	−8
2^{--}	3.71	3.93 ± 0.23		1.45	1.52 (2)	−1
3^{--}	4.03	4.13 ± 0.29		1.57	1.59 (4)	

Regge poles are not the only singularities in the complex angular momentum plane. Exchange by several reggeons in the t-channel leads to moving branch points (or Regge cuts) in the j-plane [22, 23]. The contributions of these singularities to scattering amplitudes $T_n(s,0) \sim s^{1+n\Delta}$ are especially important at high energies for $\Delta > 0$. The whole series of n-pomeron exchanges should be summed. An account of these multi-pomeron exchanges in the t-channel leads to unitarization of scattering amplitudes. The Gribov Reggeon diagram technique [36] allows one to calculate the contributions of Regge cuts to scattering amplitudes.

From the standpoint of the $1/N$-expansion, n-pomeron exchange contributions correspond to more complicated topologies with 'handles'. Each topological class of surfaces is characterized by a given number of boundaries (n_{b}) and handles (n_{h}). Topological expansion allows one to give a complete classification of diagrams and to determine their dependence on the parameter $1/N$. The diagrams of a given topological class have the following dependence on $1/N$:

$$T_{n_{\mathrm{b}}, n_{\mathrm{h}}} \sim \left(\frac{1}{N}\right)^{n_{\mathrm{b}}+2n_{\mathrm{h}}}. \tag{8}$$

Thus, the contribution of planar diagrams ($n_{\mathrm{b}} = 1$, $n_{\mathrm{h}} = 0$) to the scattering amplitude is $\sim 1/N$, the cylinder diagram ($n_{\mathrm{b}} = 2$, $n_{\mathrm{h}} = 0$) contribution is $\sim (1/N)^2$, and that of the diagram of the two-pomeron exchange ($n_{\mathrm{b}} = 2$, $n_{\mathrm{h}} = 1$) is $\sim (1/N)^4$. Equation (8) is valid for 4-point functions (amplitudes). For amplitudes with a larger number of hadrons, one should take into account that each additional external hadronic state introduces the factor $1/\sqrt{N}$ due to normalization of its wave function.

Note that the ratio of the cylinder diagram to the planar one is $\sim 1/N$; however, for amplitudes with vacuum quantum numbers in the t-channel, the cylinder-type diagrams dom-

inate at high energies, because their relative contribution increases as $s^{\alpha_P(0)-\alpha_R(0)}$ as energy increases. This is one of the manifestations of the dynamical character of the $1/N$-expansion. In many cases, the type of process (and the number of boundaries) is fixed by the quantum numbers in the t-channel. In this case, the expansion is in the number of handles and, according to Eqn (8), the expansion parameter is $(1/N)^2$, as was mentioned above.

3. High-energy hadronic interactions

The topological, or $1/N$-expansion discussed in the previous section gives a useful classification of all QCD diagrams. It becomes especially predictive if a definite space-time picture for these diagrams is given.

The process of hadronic interactions at high energies can be related to the production of new objects — color tubes or strings [9–13]. The planar diagrams in Fig. 3 can be interpreted as annihilation of the valence quarks of colliding hadrons and the formation of color tubes, which later decay into two (Fig. 3a) or several (Fig. 3b) final hadrons [14, 15]. It is possible to show that planar diagrams lead naturally to the Regge asymptotic behavior for binary processes and to derive the rules for fragmentation functions that describe the transformation of the color tube to hadrons [14, 15]. In the same way, one can relate the cylinder-type diagrams to a process of color octet exchange in the t-channel, which leads to the formation and subsequent decay of two tubes (strings) [15, 17]. Fragmentation of each string has the same properties as in the planar case.

Detailed models of the breaking of strings have been developed [12] and are now widely used in Monte Carlo simulations of multiparticle production.

Because there are two strings in the pomeron case, we conclude that the density of produced hadrons at very high energy and in the central rapidity region is in this case twice as large as in the planar case. The same follows from the comparison of the single-chain diagram in Fig. 3b with the two-chain diagram in Fig. 4b. The string model thus provides a simple picture of interaction for diagrams of the $1/N$-expansion.

In models based on the Reggeon theory and the space-time picture of $1/N$-expansion in QCD [15, 17], it is usually assumed that the pomeron corresponding to cylinder-type diagrams is a simple pole with $\alpha_P(0) > 1$. The value of $\alpha_P(0)$ is determined from the analysis of experimental data.

For such a 'supercritical' pomeron, higher terms of the topological expansion associated with the exchange by several pomerons in the t-channel are also important. This is because, although the exchange by n-pomerons is $\sim 1/(N^2)^n$, it is enhanced by the factor $(s/s_0)^{n\Delta}$. It is therefore necessary to sum many terms of the topological expansion at very high energy. The s-channel discontinuities of these diagrams are related to processes of production of $2k\,(k \leqslant n)$ chains of particles.

An important ingredient of the Reggeon approach to high-energy hadronic interactions is the AGK-cutting rules [38]. These rules define s-channel discontinuities of the n-pomeron exchange contributions and thus determine the multiparticle content of arbitrary Reggeon diagrams. In the method based on the $1/N$-expansion, these rules give us the possibility to determine the cross sections for production of $2k$ chains (strings) with any number of uncut pomerons if the contributions of all n-pomeron exchanges to the forward elastic scattering amplitude are known. These contributions can be calculated using the Reggeon diagram technique [36]. In most calculations, diagrams of the eikonal type have been taken into account [17, 15]. For example, in the 'quasieikonal' approximation (for an account of more complicated diagrams with interactions between pomerons, see below) the cross sections σ_k of the production of $2k$ chains have the form [39]

$$\sigma_k(\xi) = \frac{\sigma_P}{kz}\left[1 - \exp(-z)\sum_{i=0}^{k-1}\frac{z^i}{i!}\right], \qquad k \geqslant 1\,, \tag{9}$$

where

$$\sigma_P = 8\pi\gamma_P \exp(\Delta\xi)\,, \quad z = \frac{2C\gamma_P}{R^2 + \alpha'_P\xi}\exp(\Delta\xi)\,, \quad \xi = \ln\frac{s}{s_0}\,.$$

The quantity C accounts for the modification of the eikonal approximation due to intermediate inelastic diffractive states.

The total interaction cross section in this model has the form

$$\sigma^{\rm tot} = \sum_{n=0}^{\infty}\sigma_n = \sigma_P f\left(\frac{z}{2}\right), \quad f\left(\frac{z}{2}\right) = \sum_{n=1}^{\infty}\frac{(-z)^{n-1}}{n\cdot n!}\,, \tag{10}$$

where $\sigma_0(\xi) = \sigma^{\rm el} + \sigma^{\rm DD}$ is the cross section of diffractive processes and is given by the formula

$$\sigma_0(\xi) = \sigma_P\left[f\left(\frac{z}{2}\right) - f(z)\right]. \tag{11}$$

The simplest parameterization of the pomeron exchange has been used in Eqns (9)–(11),

$$T_P(\xi, t) = \gamma_P \exp\left[\alpha_P(0)\xi + (R^2 + \alpha'_P\xi)\,t\right]. \tag{12}$$

This model is used below for describing different aspects of high-energy hadronic interactions. The parameters of the pomeron exchange, γ_P, R^2, Δ, and α'_P, were determined from the description of experimental data on the total interaction cross sections and differential cross sections of elastic pp-, $p\bar{p}$-scattering at high energies [40, 41]. The most important parameter, Δ, is $\Delta = 0.12-0.14$ in the 'quasieikonal' approximation. We note that the value of Δ becomes larger ($\Delta \approx 0.2$) than in the 'quasieikonal' approximation if the interactions between pomerons are taken into account [42].

For super-high energies, when $\xi \gg 1$, $\sigma^{(\rm tot)}(\xi)$ has a Froissart-type behavior,

$$\sigma^{\rm tot}(\xi) \simeq \frac{8\pi\alpha'_P\Delta}{C}\,\xi^2\,. \tag{13}$$

This type of behavior for the total cross section is common for a broad class of models with $\alpha_P(0) > 1$. The slope of the diffraction cone also increases asymptotically as ξ^2.

Inclusive cross sections and multiplicity distributions can be obtained in this approach by summing over hadronic production for all processes of formation of $2k$ chains,

$$\frac{{\rm d}\sigma_c}{{\rm d}y_c} = \sum_{k=0}^{\infty}\sigma_k(\xi) f_c^k(\xi, y_c)\,, \tag{14}$$

$$\sigma_N(\xi) = \sum_{k=0}^{\infty}\sigma_k(\xi)\,W_N^k\big(\bar{N}_k(\xi)\big)\,, \tag{15}$$

where

$$f_c^k(\xi, y_c) = \frac{1}{\sigma_k} \frac{\mathrm{d}\sigma_c^k}{\mathrm{d}y_c}$$

and W_N^k are the rapidity and multiplicity distributions for the $2k$-chain production. The term with $k = 0$ in Eqns (14) and (15) corresponds to the contribution of the diffraction dissociation process σ^{DD}.

For arbitrary configurations, when there are both valence and 'sea'-chains, the functions $f_c^k(\xi, y_c)$ can be written as convolutions of distributions of quarks (ends of chains) in colliding hadrons with fragmentation functions [17, 15]. In the QGSM, all these functions can be determined theoretically and are expressed in terms of intercepts of the known Regge poles [37, 15].

Contrary to other models, where fragmentation functions are determined from experimental data, in the QGSM practically all parameters are fixed theoretically. The inclusive spectra in this model automatically have the correct triple-Regge limit as $x \to 1$ and double-Regge limit as $x \to 0$, and satisfy all conservation laws.

3.1 Comparison with experiment

Here we compare predictions of the models based on the Reggeon theory, the $1/N$-expansion in QCD, and the space-time picture of hadronic interactions discussed above with experimental data. For definiteness, the QGSM is used in what follows. After all the Pomeranchuk pole parameter are determined from the fit to experimental data on the total cross sections of pp-, $\mathrm{p\bar{p}}$-interactions and the slope of the diffraction cone in elastic pp-scattering, the predictions of the QGSM for different characteristics of multiparticle production at high energies contain practically no new free parameters.

For the n-pomeron exchange diagrams of the eikonal type (without interaction between pomerons), there is a cancellation of their contributions to the single-particle inclusive spectra in the central rapidity region for $n \geqslant 2$ [38]. Therefore, only the pole diagram makes a contribution and inclusive spectra increase with energy as $f_c^a \sim (s/s_0)^{\Delta}$. This means, in particular, that the study of the energy dependence of inclusive spectra in the central rapidity region gives more reliable information on the value of Δ than the study of σ^{tot}, for which pomeron cuts strongly modify the energy dependence compared to the pole diagram.

Rapidity (and pseudorapidity) distributions of charged particles in pp-, $\mathrm{p\bar{p}}$-interactions at different energies are shown in Fig. 5. For the 'nonenhanced' diagrams considered in this model, the inclusive cross sections $\mathrm{d}\sigma_c/\mathrm{d}y$ increase with energy as $\sim (s/s_0)^{\Delta}$ at very high energies and at $y \approx 0$. It follows from Fig. 5 that the value $\Delta = 0.12-0.14$, found from the analysis of $\sigma^{\mathrm{tot}}(s)$ [40, 41], is in perfect agreement with the growth of rapidity distributions with energy. We note that in the intermediate energy region $\sqrt{s} \sim 10$ GeV, there are important effect connected with the fluctuations of the ends of the strings, which leads to an extra increase of the inclusive spectra in the central rapidity region [14].

The integral over the rapidity distribution of the particle number density,

$$\frac{\mathrm{d}n_c}{\mathrm{d}y} = \frac{1}{\sigma^{\mathrm{in}}} \frac{\mathrm{d}\sigma_c}{\mathrm{d}y},$$

is given by the average multiplicity of charged hadrons $\langle N_{\mathrm{ch}} \rangle$. The model reproduces both rapidity distributions and $\langle N_{\mathrm{ch}} \rangle$ at accessible energies quite well [14]. $\langle N_{\mathrm{ch}} \rangle$ increases with energy faster than $\ln(s/s_0)$ and reaches values of about 70 charged particles in the LHC energy range.

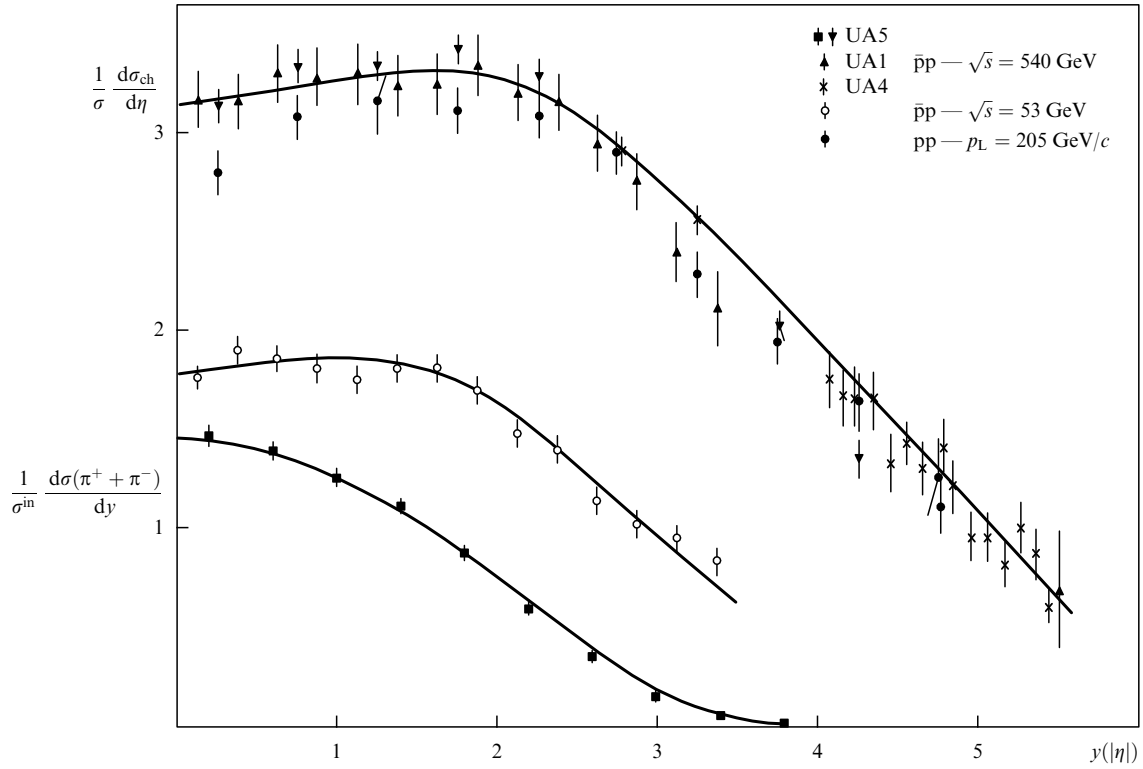

Figure 5. Rapidity distributions of charged particles in pp-, $\mathrm{p\bar{p}}$-interactions at various energies.

The multiplicity distributions in the model are given according to Eqn (15) by a sum of contributions connected to different numbers of cut pomerons ($2k$ chains). Each of these contributions has a Poisson-like form (only short-range correlations inside chains), but their sum has a very peculiar dependence on energy. At energies $\sqrt{s} \leqslant 10^2$ GeV, different contributions overlap strongly. This leads to an approximate KNO scaling (the dependence on only $N_{\rm ch}/\langle N_{\rm ch}\rangle$). The model reproduces multiplicity distributions at these energies [14] quite well. The mean number of chains increases with energy [as $(s/s_0)^{\Delta}$] and the model predicts [14] a certain violation of the KNO scaling. This prediction was confirmed by the experimental data at the $S\bar{p}pS$-collider (Fig. 6). In this figure, the multiplicity distribution at energy $\sqrt{s} \sim 10^5$ GeV is also shown. As energy increases, the maximum of the distribution in the variable $z = N_{\rm ch}/\langle N_{\rm ch}\rangle$ moves to the left and the distribution increases in the region of large z. It is interesting to note that at super-high energies $\sqrt{s} \sim 10^5$ GeV, different terms in the sum in Eqn (15) start to separate and the distribution has the corresponding maxima and minima. At the accessible energies $\sqrt{s} \leqslant 10^3$ GeV, only the first maximum and a 'shoulder' start to appear. This prediction of a structure in multiplicity distributions at very high energies is consistent with experimental observations at existing colliders.

The model also reproduces the semi-inclusive rapidity distributions and dependence of multiplicity distributions on rapidity [14] quite well. Thus, the study of multiplicity distributions not only confirms the multi-component structure of the model, but also shows that the weights of different components ($\sigma_k/\sigma^{\rm in}$) are close to the predictions of the quasi-eikonal approximation.

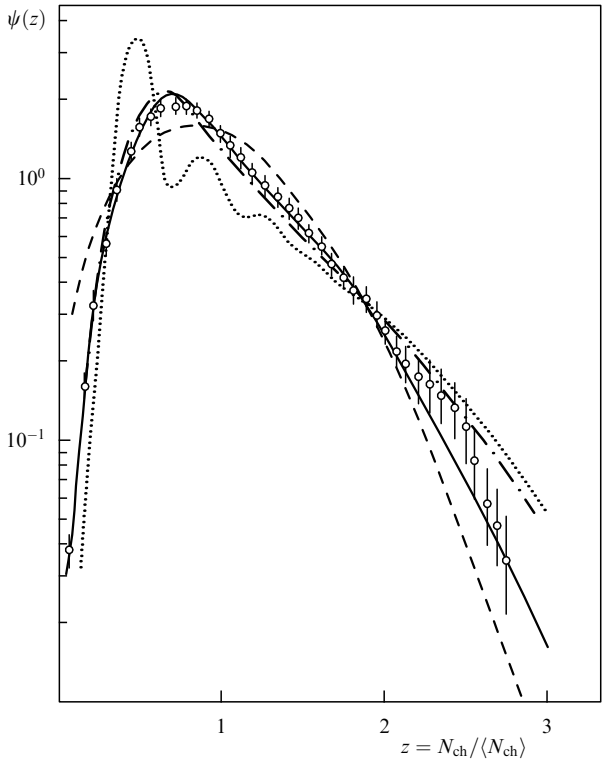

Figure 6. KNO distributions in pp-, $p\bar{p}$-interactions. The solid curve is for $\sqrt{s} = 540$ GeV, the dotted curve is for $\sqrt{s} = 10^5$ GeV, and the dashed curve represents the data for $\sqrt{s} \sim 10$ GeV. The data at $\sqrt{s} = 540$ GeV are from the UA5 group.

Another consequence of the multi-pomeron contributions is the existence of the long-range rapidity correlations. This leads, in particular, to a large long-range part of the correlation function $C(y, 0)$, which rapidly increases with energy [as $s/s_0)^{2\Delta}$], and to strong forward – backward correlations. For a single pomeron contribution, the correlations are of a short-range order in rapidity, but due to the presence of several components with different densities of produced particles, the long-range correlations become important. In the case of forward – backward correlations, for example, by increasing the number of particles in the forward hemisphere, we automatically increase the number of produced chains and thus increase the mean multiplicity of hadrons in the backward hemisphere. The dependence of the mean multiplicity of charged hadrons produced in the backward hemisphere (rapidity region from -4 to -1) on the number of charged particles in the forward rapidity interval (1 to 4) is shown in Fig. 7. The model reproduces the nearly linear dependence of the experimental data.

We now consider inclusive spectra of different hadrons at high energies. The QGSM gives us the possibility to calculate spectra for all values of the variable x [14]. As an example, the spectra of π^+-mesons in pp-interactions are shown in Fig. 8. Note that the Feynman scaling is strongly violated in the region of small x. On the other hand, in the fragmentation region for $x \geqslant 0.1$, the scaling violation is rather weak. This has important implications for cosmic ray experiments.

The model predictions for inclusive cross sections and mean multiplicities of $K^{\pm}$-, K^0-, and $\bar{K}^0$-mesons are presented in Ref. [43] and are in good agreement with experimental data. In the QGSM, the strange quark suppression factor is predicted theoretically [37] and is confirmed by experimental data. The ratio of the mean multiplicities of kaons and pions increases with energy. This increase in the model is mainly due to the mass difference of kaons and pions and the ratio tends to a constant value ≈ 0.12 asymptotically.

The spectra of the 'leading' particles like protons and neutrons are well described in the QGSM [43]. The spectra of the protons have a clear 'leading' behavior (distributed in the region $x \sim 1$) due to the fragmentation of diquarks, which have a distribution concentrated at x_{qq} close to 1. The

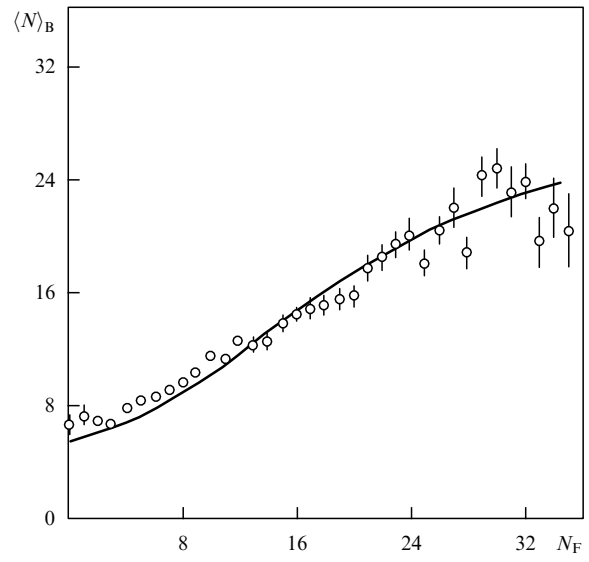

Figure 7. Forward – backward correlations at $\sqrt{s} = 540$ GeV.

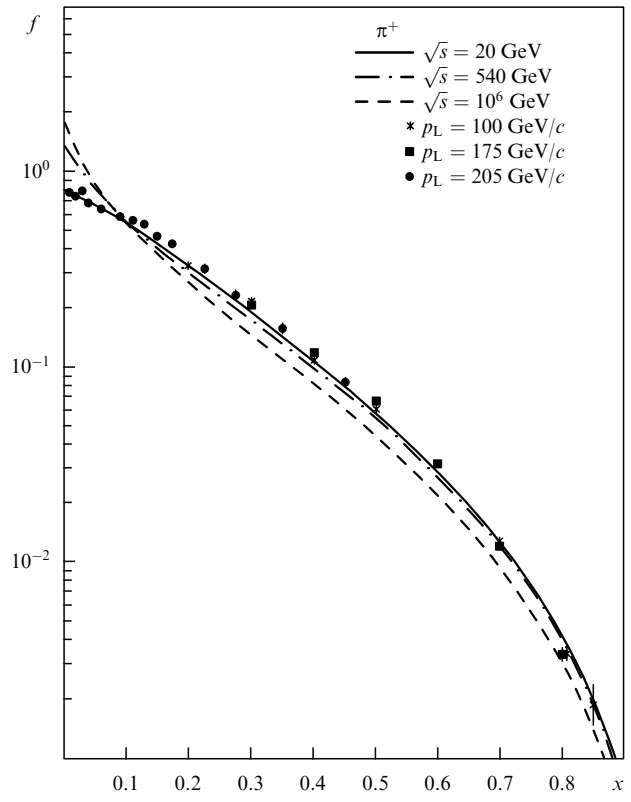

Figure 8. Inclusive cross sections for π^+ in pp-collisions at various energies.

antiprotons, on the contrary, are determined mainly by the 'central' production in the valence chains and also arise from sea chains. Asymptotically, in the central region ($x \approx 0$), the spectra of protons and antiprotons should be equal (the same is true for all particles and antiparticles).

Another example of the 'leading' behavior is the spectrum of Λ-hyperons, shown in Fig. 9. The strange-quark suppression in the fragmentation function of the model is a function

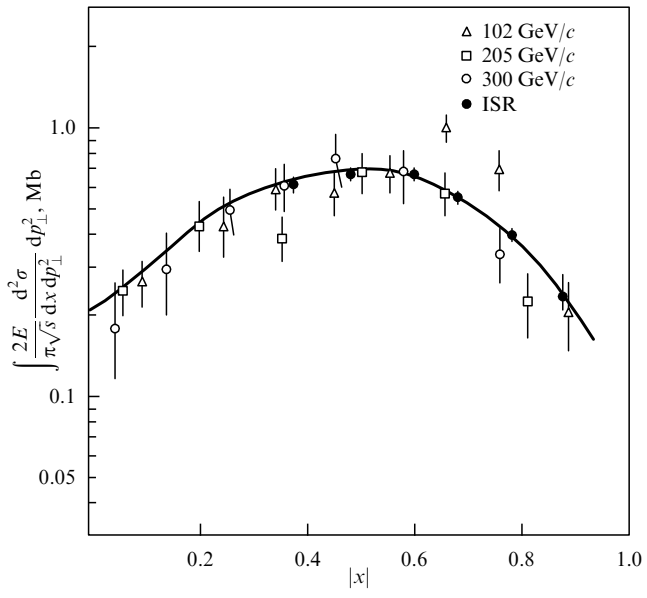

Figure 9. Spectra of Λ-hyperons.

of z and is proportional to

$$(1-z)^{\alpha_\rho(0)-\alpha_\varphi(0)}$$

as $z \to 1$. This leads to a shift of the maximum of the spectrum for Λ to smaller values of x than for nonstrange baryons (like n or Δ-isobar), in good agreement with experimental data.

The model was extended to the processes of charmed particle production in Ref. [44]. The main problem is here a poor knowledge of the $c\bar{c}$-trajectory. The form of the x-behavior and absolute normalization depend strongly on the intercept of the $c\bar{c}$-trajectory. In Ref. [44], two values of $\alpha_{c\bar{c}}(0)$ have been used: $\alpha_{c\bar{c}} = -2$, which follows from the mass spectrum under the assumption of linear trajectories, and $\alpha_{c\bar{c}} = 0$, from perturbative calculations. The nonperturbative value is preferable from the analysis of recent data on Λ_c-production. The model predictions for the energy behavior and the form of inclusive spectra of various charmed particles are in reasonable agreement with experiment [45, 46].

The QGSM thus gives a completely adequate description of the main features of multiparticle production of hadrons at high energies. Monte Carlo realizations of the model also exist [47]. A similar quality of description of the data is achieved in the DPM [17].

At the end of this section, we give a short summary of the model predictions for the LHC energy $\sqrt{s} = 14$ TeV. The total pp-interaction cross section is predicted to be equal to 103 – 106 mb, while the total elastic cross section should be close to 26 – 28 mb. The diffraction cone slope is predicted to be $B = 21.5$ GeV^{-2}. The total inelastic diffractive cross section is close to 25 mb. Thus, the total cross section of all diffractive channels is close to half the total interaction cross section. In the QGSM, the density of charged hadrons in the central rapidity region $\mathrm{d}n_{\mathrm{ch}}/\mathrm{d}y = 5.5$ and the total multiplicity of charged hadrons is equal to 70 at LHC .

3.2 Diffractive production processes and interactions between pomerons

In Gribov's Reggeon theory, contributions of rescatterings (multi-pomeron cuts) are closely connected to cross sections of diffractive processes. In the eikonal approximation, only elastic rescatterings are taken into account. In general, inelastic diffractive processes should also be taken into account. In the 'quasieikonal' approximation considered above, diffractive dissociation of colliding hadrons is also taken into account under some simplifying assumptions. We now consider diffractive production of particles at high energies in more detail.

In the Regge pole model, these processes are described by the diagrams with a pomeron exchange in the t-channel. It is possible to have excitation of one of the colliding hadrons (single diffraction dissociation, Fig. 10a) or excitation of both initial particles (double diffraction dissociation, Fig. 10b).

All the diffractive processes are characterized by a large rapidity gap between groups of produced particles. For example, for single diffraction dissociation, there is a gap between the particle $1'$ and the rest of the system of hadrons. This rapidity gap $\Delta y \approx \ln(1/(1-x))$, where x is the Feynman x for hadron $1'$. The mass of a diffractively excited state at a high energy s can be large. The only condition for diffraction dissociation is $s_i \ll s$. For large masses of the excited states, $s_2 \approx (1-x)s$ and $\Delta y \approx \xi' = \ln(s/s_2)$.

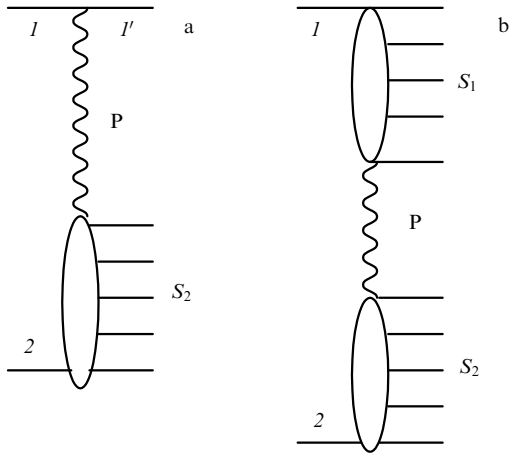

Figure 10. Diagrams for diffractive production of hadrons in the Regge pole model.

The cross section for inclusive single diffraction dissociation in the Regge pole model can be written as

$$\frac{\mathrm{d}^2\sigma}{\mathrm{d}\xi_2\,\mathrm{d}t} = \frac{(g_{11}(t))^2}{16\pi}\left|G_{\mathrm{P}}(\xi',t)\right|^2\sigma_{\mathrm{P2}}^{\mathrm{tot}}(\xi_2,t)\,, \tag{16}$$

where $\xi_2 \equiv \ln(s_2/s_0)$ and $G_{\mathrm{P}} = \eta(\alpha_{\mathrm{P}}(t))\exp[(\alpha_{\mathrm{P}}(t)-1)\xi']$ is the pomeron Green function. The quantity $\sigma_{\mathrm{P2}}^{\mathrm{tot}}(\xi_2,t)$ can be considered as the pomeron – particle total interaction cross section [48]. Note that this quantity is not directly observable and is defined by relation (16). This definition is useful, however, because at large s_2, $\sigma_{\mathrm{P2}}^{\mathrm{tot}}$ has the same Regge behavior as the usual cross sections,

$$\sigma_{\mathrm{P2}}^{\mathrm{tot}}(s_2,t) = \sum_k g_{22}^k(0)\,r_{\mathrm{PP}}^{\alpha_k}(t)\left(\frac{s_2}{s_0}\right)^{\alpha_k(0)-1}, \tag{17}$$

where the $r_{\mathrm{PP}}^{\alpha_k}(t)$ is the triple-Reggeon vertex, which describes the coupling of two pomerons to the Reggeon α_k.

In this kinematical region $s \gg s_2 \gg m^2$, the inclusive diffractive cross section is described by the triple-Regge diagrams (Fig. 11) and has the form

$$f = \sum_k G_k(t)(1-x)^{\alpha_k(0)-2\alpha_{\mathrm{P}}(t)}\left(\frac{s}{s_0}\right)^{\alpha_k(0)-1}. \tag{18}$$

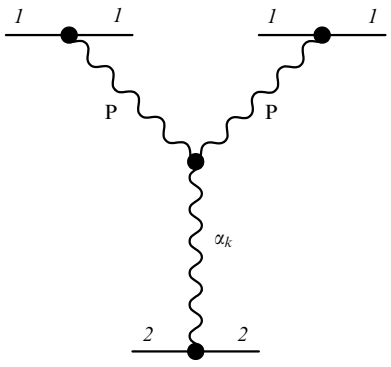

Figure 11. Triple-Regge diagram.

The Pomeron – proton total cross section and triple-Regge vertices $r_{\mathrm{PP}}^{\mathrm{P}}$, r_{PP}^{f} have been determined from the analysis of experimental data on diffractive production of particles in hadronic collisions (see [49]).

In the eikonal-type models (e.g., 'quasieikonal') discussed above, the diffraction dissociation to states with not too large masses has been taken into account. Diffractive production of states with large masses is related to diagrams with interaction between pomerons. In the first approximation, disregarding these interactions is justified by the smallness of triple-pomeron and 4-pomeron interaction vertices, found from the analysis of diffractive processes [49]. But at very high energies, it is necessary to include all these diagrams in order to have a self-consistent description of high-energy hadronic interactions, including large-mass diffractive production of particles. It was demonstrated in [42] that inclusion of these diagrams leads in many cases to predictions that are very close to the results of eikonal-type models; however, the value of the 'bare' pomeron intercept increases up to $\alpha_{\mathrm{P}}(0) \approx 1.2$. We demonstrate below that an account of interactions between pomerons is important for heavy ion collisions at high energies and these effects are seen experimentally at RHIC.

4. Pomeranchuk theorem and 'odderon'

Crossing and analyticity of scattering amplitudes also lead to interesting relations between the asymptotic behavior of scattering amplitudes for particles and antiparticles. Pomeranchuk [2] has shown that dispersion relations for the forward scattering amplitudes with the natural extra assumptions:

(a) amplitudes do not oscillate as $s \to \infty$;

$$\text{(b)}\ \frac{|\mathrm{Re}\,T(s,0)|}{\mathrm{Im}\,T(s,0)}\,\frac{1}{\ln s} \to 0 \quad \text{for} \quad s \to \infty\,;$$

lead to an important asymptotic relation between the total interaction cross sections for particles and antiparticles,

$$\sigma_{ab}^{\mathrm{tot}} = \sigma_{\bar{a}b}^{\mathrm{tot}}\,, \qquad s \to \infty\,. \tag{19}$$

Note that assumption (b) cannot be proved from general properties of analyticity and unitarity. In the case where total cross sections increase with energy, it is possible to prove the following extension of the Pomeranchuk theorem:

$$\frac{\sigma_{ab} - \sigma_{\bar{a}b}}{\sigma_{ab} + \sigma_{\bar{a}b}} \to 0\,, \qquad s \to \infty\,. \tag{20}$$

In the Reggeon theory, the Pomeranchuk theorem is automatically satisfied if the leading Regge singularity (pomeron) has vacuum quantum numbers. In this case, differences of cross sections for particles and antiparticles decrease as powers of s for $s \to \infty$,

$$\Delta\sigma(s) = \sigma_{ab}(s) - \sigma_{\bar{a}b}(s) = \sum_i g_i(0)\left(\frac{s_0}{s}\right)^{(1-\alpha_i(0))}, \tag{21}$$

where the sum is over poles with negative signature and C-parity (ω, ρ).

The existing data on $\Delta\sigma(s)$ are in perfect agreement with the prediction of the Reggeon approach and do not indicate any violation of the Pomeranchuk theorem (Fig. 12).

A singularity in the j-plane with negative signature and C-parity and an intercept close to unity ('odderon') [50], which could lead to a violation of the Pomeranchuk theorem, appears in the QCD perturbation theory [51]. It is

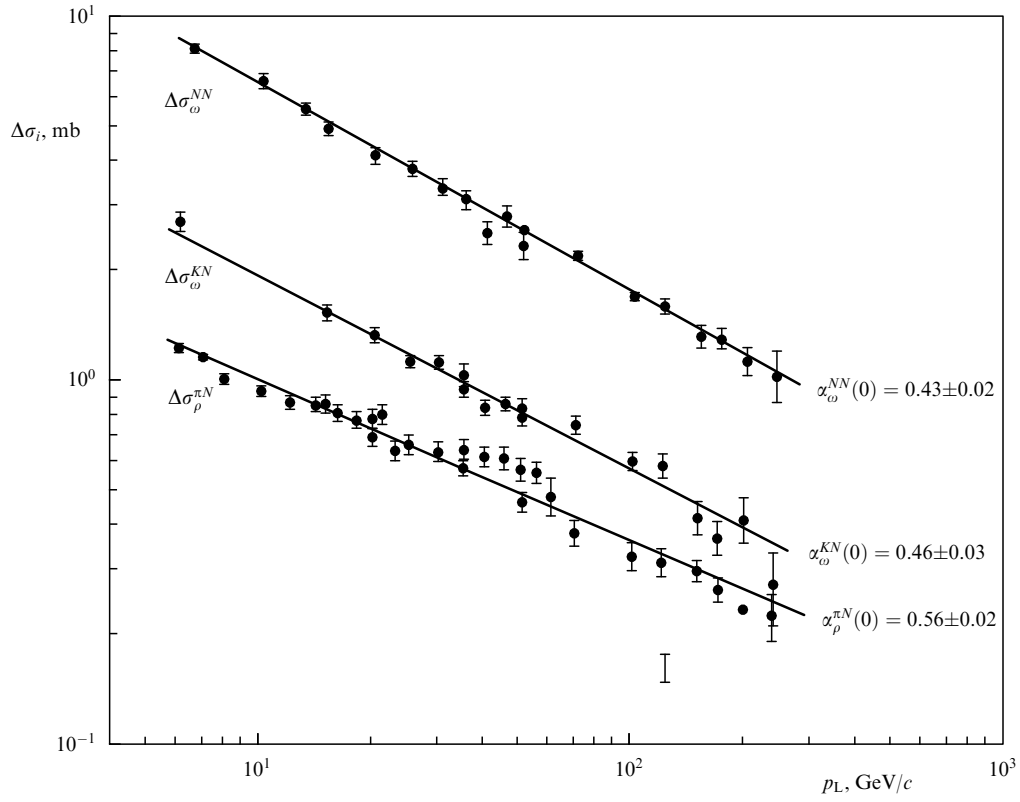

Figure 12. Differences in the total cross sections $\Delta\sigma_i$ and their description in the Regge pole model.

a bound state of three reggeized gluons. In the approach described above, which takes nonperturbative effects into account [33], the lowest state made of three gluons connected by strings with quantum numbers 3^{--} has a rather large mass ($M \approx 4$ GeV) and the leading Regge trajectory with negative signature and C-parity has a very low intercept $\alpha_{3g}(0) < -1$. Contrary to the pomeron case, its mixing with $q\bar{q}$ trajectories (ω, φ) is weak in the small-t region, and there is no 'odderon' in this approach. Thus, the experimental search for the 'odderon' in the small-t region is very important for understanding the dynamics of j-plane singularities in QCD.

5. Pomeron and small-x physics

5.1 Diffraction processes in deep inelastic scattering

In this section, we show that the methods developed for the analysis of high-energy hadronic interactions described above can be applied to the physics of small Bjorken x studied in deep inelastic scattering.

Experiments at HERA have found two extremely important properties of small-x physics: a fast increase of parton densities as x decreases [53, 54] and the existence of substantial diffractive production in deep inelastic scattering (DIS) [55, 56].

In DIS, it is possible to study different asymptotic limits. In the region

$$Q^2 \to \infty \quad \text{and} \quad x = \frac{Q^2}{W^2 + Q^2} \sim 1 \quad \left(W^2 = (p_{\gamma^*} + p_{\mathrm{p}})^2\right),$$

the usual QCD evolution equations of parton distributions can be applied and the structure functions can be predicted if the initial conditions for structure functions at $Q^2 = Q_0^2$ are formulated. On the other hand, if Q^2 is fixed and $x \to 0$ (or $\ln(1/x) \to \infty$), the asymptotic Regge limit is relevant. The most interesting question is: what is the behavior of DIS in the region where both $\ln(1/x)$ and $\ln(Q^2)$ are large? This is a transition region between perturbative and nonperturbative dynamics in QCD and its study can give important information on the properties of confinement and its relation to the QCD perturbation theory. The asymptotic Regge behavior in the Regge region of DIS is usually described in terms of the Pomeranchuk singularity and is therefore related to the behavior of hadronic interactions at high energies.

A fast increase of $\sigma_{\gamma^*\mathrm{p}}^{\mathrm{tot}}$ as $W^2 \equiv s$ increases at large Q^2 observed experimentally [53, 54] raises the question whether there are two different pomerons — 'soft' and 'hard'. Investigation of the dynamical origin of the pomeron in QCD described above [33] shows that there are no theoretical reasons for such a situation, and the rightmost pole in the j-plane is most probably generated by both 'soft' and 'hard' dynamics. It is assumed in what follows that there is one ('physical') pomeron pole with the same $\alpha_{\mathrm{P}}(0)$ in all processes; that is, the P-pole in DIS is the same as in hadronic processes. On the other hand, the effective intercept, which depends on the relative contribution of multi-pomeron diagrams, can be different in different processes.

There are good reasons to believe that the fast increase of the Reggeon $\sigma_{\gamma^*\mathrm{p}}^{\mathrm{tot}}$ with energy in the HERA energy range will change to a slower increase at much higher energies. In the Reggeon theory, this is related to multi-pomeron branching. In the parton picture, these effects can be described as shadowing in highly dense systems of partons, with the eventual 'saturation' of densities occurring in the limit as $x \to 0$. This problem has a long history (see [57] for reviews)

and has been extensively discussed recently [58]. It is closely related to the problem of the dynamics of high-energy heavy ion collisions [59] (see below).

It was suggested in [60] that the increase of the effective intercept of the pomeron, $\alpha_{\rm eff} = 1 + \Delta_{\rm eff}$, as Q^2 increases from zero to several GeV^2 is mostly due to a decrease of shadowing effects with increasing Q^2. A good description of all existing data on the γ^*p total cross sections in the region $Q^2 \leqslant 5-10$ GeV^2 was obtained in [60, 61] using the parameterization of $\Delta_{\rm eff}(Q^2)$ given by

$$\Delta_{\rm eff}(Q^2) = \Delta_0\left(1 + \frac{2Q^2}{d+Q^2}\right),$$

where d is the parameter that determines the values of Q^2 interpolating $\Delta_{\rm eff} = \Delta_0 \approx 0.1$ at $Q^2 = 0$ and $\Delta_{\rm eff} \approx 0.2$ at large for Q^2. The latter value is close to Δ determined from the analysis of hadron interactions at high energies. QCD evolution effects must be taken into account for $Q^2 > 5-10$ GeV^2. Using the above parameterization as the initial condition in the QCD evolution equation, it is possible to describe the data in the whole region of Q^2 studied at HERA [60, 62].

As emphasized above, the value of $\Delta_{\rm eff}$ should depend not only on Q^2 but also on x and should decrease as $x \to 0$. It is important to build an explicit model based on the Reggeon theory where all these effects are incorporated.

This problem was investigated in [63], where the Reggeon approach was applied to the processes of diffractive γ^*p interaction. It was emphasized in the previous section that in the Reggeon calculus, the amount of rescatterings (or multipomeron exchanges) is closely related to diffractive production. AGK-cutting rules [38] allow us to calculate the cross-section of inelastic diffraction if the contributions of multipomeron exchanges to the elastic scattering amplitude are known. It is therefore very important for the self-consistency of theoretical models to describe not only the total cross sections, but also the inelastic diffraction. In [63], an explicit model for the contribution of rescatterings was constructed that leads to the pattern of energy behavior of $\sigma^{\rm tot}_{\gamma^*{\rm p}}(W^2, Q^2)$ for the various Q^2 as described above. Moreover, it allows us to simultaneously describe diffraction production by real and virtual photons. In this model, it is possible to study the regime of 'saturation' of parton densities quantitatively.

We now briefly discuss the qualitative picture of diffractive dissociation of a highly virtual photon at high energies. It is convenient to discuss this process in the laboratory system, where the quark – gluon fluctuations of a photon live a long time, $\sim 1/x$ [64]. A virtual photon fluctuates first to a $q\bar{q}$ pair. There are two different types of configurations of such pairs, depending on the transverse distance between quarks (or $k_\perp$):

(a) Small-size configurations with $k_\perp^2 \sim Q^2$. These small dipoles ($r \sim 1/k_\perp \sim 1/Q$) have a small ($\sim r^2$) total interaction cross section with the proton.

(b) Large-size configurations with $r \sim 1/\Lambda_{\rm QCD}$ and $k_\perp \sim \Lambda_{\rm QCD} \ll Q$. They have a large total interaction cross section, but their phase space is small at large Q^2, because these configurations are kinematically possible only if the fraction of the longitudinal momentum carried by one of the quarks is very small, $x_1 \sim k_\perp^2/Q^2 \ll 1$. This configuration corresponds to the 'aligned jet', introduced by Bjorken and Kogut [65].

Both configurations lead to the same behavior of $\sigma^{\rm tot}_{\gamma^*{\rm p}} \sim 1/Q^2$, but they behave differently in the process of the diffraction dissociation of a virtual photon [66, 67]. The cross section of such a process is proportional to the square of the modulus of the corresponding diffractive amplitude and is small for a small-size configuration ($\sim 1/Q^4$). For large-size configurations, the smallness is due only to the phase space, and the inclusive cross section for diffractive dissociation of a virtual photon decreases as $1/Q^2$, i.e., in the same way as the total cross section. This is true only for the total inclusive diffractive cross section, where characteristic masses of the produced states are $M^2 \sim Q^2$. For exclusive channels with fixed mass (for example, production of vector mesons) or for the longitudinal part of diffractive production, the situation is different and these cross sections decrease faster than $1/Q^2$ at large Q^2.

Inclusive diffractive production of very large masses ($M^2 \gg Q^2$) can be described in the first approximation by triple-Regge diagrams [68]. From the standpoint of the quark – gluon fluctuation of the fast photon, triple-pomeron contribution corresponds to diffractive scattering of a very slow (presumably, gluonic) parton with a small virtuality.

Model [63] uses the picture of diffraction dissociation of a virtual photon described above and is a natural generalization of models used for the description of high-energy hadronic interactions. The interaction of the small-size component in the wave function of a virtual photon is calculated using the QCD perturbation theory [67]. The main parameter of the model — the intercept of the pomeron — was fixed from a phenomenological study of hadronic interactions discussed above ($\Delta_{\rm P} = 0.2$) and was found to give a good description of γ^*p-interactions in a broad range of Q^2 ($0 \leqslant Q^2 < 10$ GeV^2). Another important parameter of the theory, the triple-pomeron vertex, obtained from a fit to the data ($r^{\rm P}_{\rm PP}/g^{\rm P}_{\rm pp}(0) \approx 0.1$), is also in reasonable agreement with the analysis of soft hadronic interactions [42, 68]. The description of the structure function F_2 as a function of x for different values of Q^2 is shown in Fig. 13 (experimental data are from H1 [53], ZEUS [54]). Diffraction dissociation of a virtual photon is usually represented as a function of Q^2, M^2 (or $\beta = Q^2/(M^2+Q^2)$), and $x_{\rm P} = x/\beta = (M^2+Q^2)/(W^2+Q^2)$. Description of HERA data on diffractive dissociation [56] in the model is shown in Figs 14 and 15. The model can be used to predict structure functions and partonic distributions at higher energies or smaller x, which will be accessible for experiments at LHC.

5.2 Shadowing effects for nuclear structure functions

The study of the shadowing effects for structure functions of nuclei in the small-x region provides a stringent test of the Reggeon approach to the small-x problem. The shadowing effects are enhanced for nuclei ($\sim A^{1/3}$) and lead to deviations from the A^1 behavior for structure functions of nuclei. The Glauber – Gribov [69, 70] approach to interactions of particles with nuclei allows us to calculate rescattering corrections for interaction of a virtual photon with a nucleus in terms of diffractive interaction of a photon with a nucleon, which was considered above.

The contribution of the double rescattering term to σ_{γ^*A} is directly expressed in terms of the differential cross section for the diffraction dissociation of a virtual photon in γ^*N-interactions,

$$\sigma^{(2)} = -4\pi\int {\rm d}^2b\, T_A^2(b)\int {\rm d}M^2\,\frac{{\rm d}^3\sigma^{\rm DD}_{\gamma^*N}(t=0)}{{\rm d}M^2\,{\rm d}t}\,F_A(t_{\rm min}), \quad (22)$$

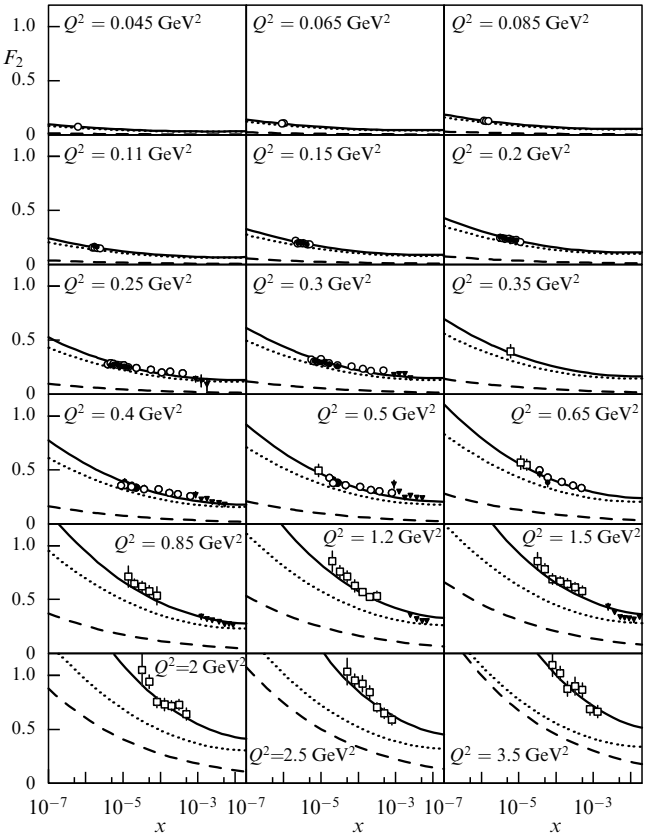

Figure 13. The structure function of a proton F_2 as a function of x for different values of Q^2 compared with experimental data. Dashed lines denote small-distance contributions and dotted lines large distance ones.

where $F_A(t_{\min}) = \exp(R_A^2 t_{\min}/3)$, $t_{\min} \approx -m_N^2 x_P^2$, and $T_A(b)$ is the nuclear profile function ($\int T_A(b)\,\mathrm{d}^2b = A$).

Higher-order rescatterings are model-dependent; in the generalized Schwimmer model [71], the ratio of the nucleus structure function to the nucleon structure function is expressed as

$$\frac{F_{2A}}{F_{2N}} = \int \frac{T_A(b)}{1 + F(x,Q^2)T_A(b)}\,\mathrm{d}^2b\,, \tag{23}$$

$$F(x,Q^2) = 4\pi \int \frac{\mathrm{d}^3\sigma^{\mathrm{DD}}_{\gamma^*N}(t=0)}{\mathrm{d}M^2\,\mathrm{d}t}\,\frac{F_A(t_{\min})}{\sigma_{\gamma^*N}(x,Q^2)}\,\mathrm{d}M^2$$

in the region of small x.

Theoretical predictions [72] based on Eqn (23) and the model for diffraction dissociation in Ref. [68] are in very good agreement with NMC group data on nuclear structure functions at very small x [73]. We believe that this approach gives reliable predictions for nuclear shadowing effects in the region of small x not yet studied experimentally. This region will play an important role in the dynamics of heavy ion collisions at super-high (LHC) energies.

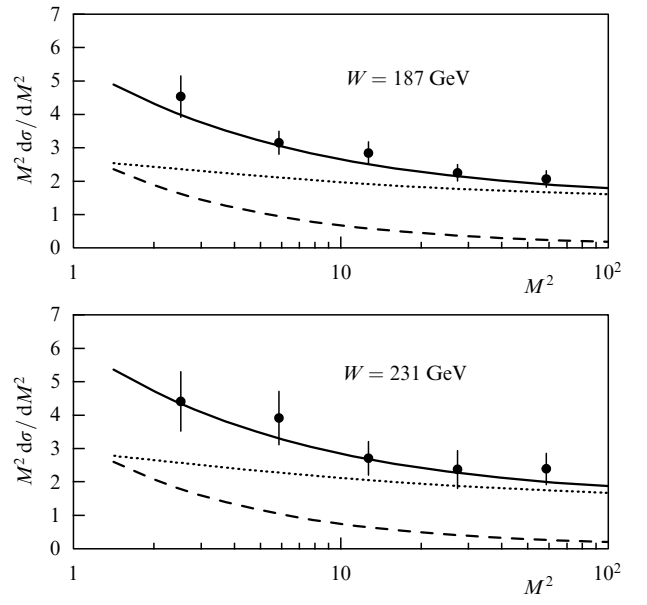

Figure 14. Cross section $M^2\,\mathrm{d}\sigma/\mathrm{d}M^2$ (in μb) for diffraction dissociation of a photon at $Q^2 = 0$ as a function of M^2 (in GeV^2).

6. Heavy-ion collisions at high energies

6.1 High-energy interactions of hadrons with nuclei

We first consider high-energy hadron–nucleus interactions. In the Glauber–Sitenko (GS) [69] model, the elastic scattering amplitude corresponds to successive rescatterings of the initial hadron on nucleons of the nucleus.

But as was emphasized by Gribov [70], the space-time picture of the interaction at high energy $E > m_h(\mu R_A)$ (μ is a characteristic hadronic scale ~ 1 GeV and R_A is the radius of the nucleus) is completely different from the picture of successive rescatterings. It corresponds to coherent interactions of a fluctuation of the initial hadron, which is 'prepared' long before its interaction with the nucleus. Nevertheless, the elastic hA-amplitude can be written as a sum of the diagrams with elastic rescatterings, which give the same result as the GS model, plus all possible diffractive excitations of the initial hadron. At not too high energies, $E_{\mathrm{L}} \sim 10^2$ GeV, these inelastic contributions lead to corrections to the GS approximation of 10–20% for the total hA cross section. But at very high energies and for inclusive cross sections, this modification of the GS approximation is very important. The difference between the GS model and Gribov's theory is essential for understanding shadowing corrections for structure functions of nuclei, as was shown in the previous section, and for many aspects of multiparticle production on nuclei [74].

An important consequence of the space-time structure of high-energy interactions of hadrons with nuclei is the AGK result [38] that for inclusive cross sections, all rescatterings cancel and these cross sections are determined by diagrams of the impulse approximation. We note that this result is only valid asymptotically in the central rapidity region for GS-type diagrams, i.e., in the case where masses of the intermediate states in rescattering diagrams are limited and do not increase with energy. The inclusive cross section for the production of a hadron a is then expressed, for a given impact parameter b, in terms of the inclusive cross section for hN interactions,

$$E\,\frac{\mathrm{d}^3\sigma^a_{hA}(b)}{\mathrm{d}^3p} = T_A(b)E\,\frac{\mathrm{d}^3\sigma^a_{hN}}{\mathrm{d}^3p}\,. \tag{24}$$

After integration over b, we obtain

$$E\,\frac{\mathrm{d}^3\sigma^a_{hA}}{\mathrm{d}^3p} = AE\,\frac{\mathrm{d}^3\sigma^a_{hN}}{\mathrm{d}^3p}\,. \tag{25}$$

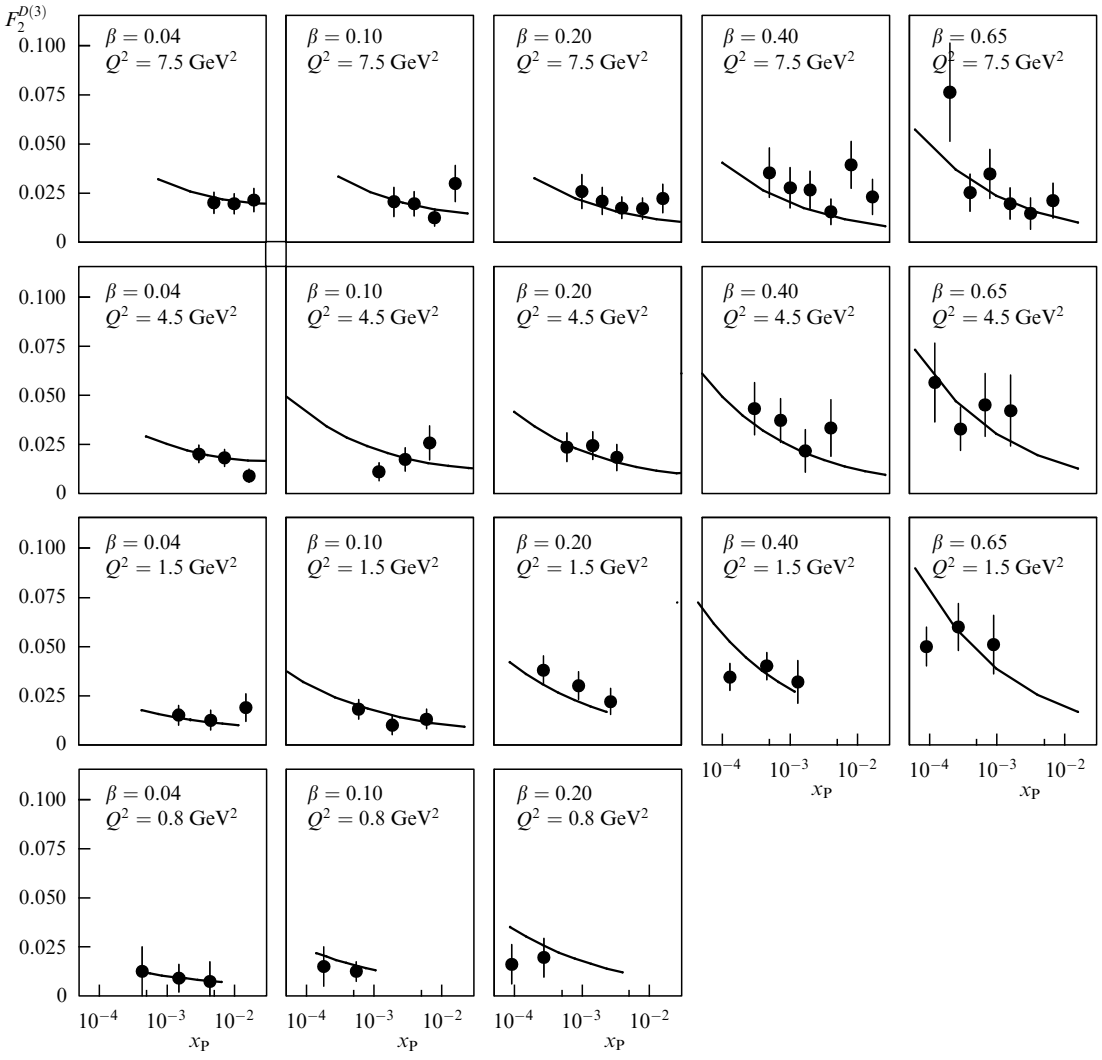

Figure 15. The diffractive structure function $F_2^{D(3)}$ as a function of x_P for fixed values of Q^2 and $\beta = Q^2/(Q^2 + M^2)$.

6.2 Particle densities in heavy-ion collisions at super-high energies

Reviews of applications of the Glauber – Gribov approach, $1/N$-expansion in QCD, and the string model to processes of nucleus – nucleus interactions can be found in Refs [17, 75].

We now consider particle densities in heavy-ion collisions in more detail.

For nucleus – nucleus collisions in the GS approximation, the AGK cancellation theorem is valid. In this case, the inclusive cross sections can be written as

$$E\,\frac{\mathrm{d}^3\sigma^a_{AB}(b)}{\mathrm{d}^3p} = T_{AB}(b)E\,\frac{\mathrm{d}^3\sigma^a_{NN}}{\mathrm{d}^3p}\,, \tag{26}$$

where $T_{AB}(b) = \int T_A(\mathbf{s})T_B(\mathbf{b}-\mathbf{s})\,\mathrm{d}^3s$. After integration over b, Eqn (26) gives

$$E\,\frac{\mathrm{d}^3\sigma^a_{AB}}{\mathrm{d}^3p} = ABE\,\frac{\mathrm{d}^3\sigma^a_{NN}}{\mathrm{d}^3p}\,. \tag{27}$$

The densities of charged particles can be obtained from Eqns (26) and (27) by dividing them by the total inelastic cross section of the nucleus – nucleus interaction. For example,

$$\frac{\mathrm{d}n^{\mathrm{ch}}_{AB}(b)}{\mathrm{d}y} = \frac{T_{AB}(b)}{\sigma^{\mathrm{in}}_{AB}}\,\frac{\mathrm{d}\sigma^{\mathrm{ch}}_{NN}}{\mathrm{d}y}\,, \tag{28}$$

$$\frac{\mathrm{d}n^{\mathrm{ch}}_{AB}}{\mathrm{d}y} = \frac{AB}{\sigma^{\mathrm{in}}_{AB}}\,\frac{\mathrm{d}\sigma^{\mathrm{ch}}_{NN}}{\mathrm{d}y}\,. \tag{29}$$

Equation (29) for particle densities integrated over the impact parameter (minimum bias events) can be rewritten as

$$\frac{\mathrm{d}n^{\mathrm{ch}}_{AB}}{\mathrm{d}y} = n_{AB}\,\frac{\mathrm{d}n^{\mathrm{ch}}_{NN}}{\mathrm{d}y}\,, \tag{30}$$

where $n_{AB} = AB\sigma^{\mathrm{in}}_{NN}/\sigma^{\mathrm{in}}_{AB}$. This corresponds to the average number of collisions in the GS model. For $A = B \gg 1$, n_{AB} behaves as $CA^{4/3}$ with $C \approx \sigma^{\mathrm{in}}_{NN}/(4\pi R_0^2)$ $(R_A = R_0A^{1/3})$. Equations (26) and (27) are usually applied to hard processes, but in the GS approximation they are valid for soft processes as well. We see below that for both soft and hard processes, these equations have to be modified.

Using Eqns (29) and (30), we obtain for Pb – Pb collisions at LHC at $y = 0$ that $\mathrm{d}n^{\mathrm{ch}}/\mathrm{d}y = 2100$ for minimum bias events and $\mathrm{d}n^{\mathrm{ch}}/\mathrm{d}y = 8500$ for central ($b < 3$ F) collisions.

Thus, the GS approximation predicts very large densities of charged hadrons in central heavy-ion collisions at LHC. But are these predictions realistic? To answer this question, we consider possible limitations of the GS approximation and also the corrections to the AGK cancellation theorem that are important at high energies.

There are two types of corrections to Eqns (24) and (26).

(a) The effects due to energy-momentum conservation: the energy of the initial hadron is shared by 'constituents' and each subcollision occurs at a smaller energy. These effects are very important in the fragmentation regions of colliding hadrons (or nuclei) and reduce particle densities. For $y = 0$, this reduction decreases as $(1/s)^{1/4}$. It is very important at SPS energies and has some effect at RHIC, but is unessential at LHC energies.

(b) Another dynamical effect is important at very high energies when diffractive production of very heavy hadronic states ($M^2 \gg m_N^2$) becomes possible. It is related to the triple-pomeron interaction discussed above and corresponds to the interaction between pomerons (strings in the string models of particle production). Because the total and inelastic cross sections of the hA- and AB-interactions at high energies are close to a black disc limit due to eikonal-type diagrams, these extra interactions have small effect on the total cross sections. But they are very important for inclusive spectra in the central rapidity region [74], where contributions of GS rescatterings cancel due to AGK rules.

Extra shadowing effects related to these interactions modify the A-dependence of the GS approximation for inclusive spectra [Eqns (24), (26)] such that the behavior $\mathrm{d}\sigma_{AB}/\mathrm{d}y \sim AB$ of the GS approximation changes to $\mathrm{d}\sigma_{AB}/\mathrm{d}y \sim A^{\alpha}B^{\alpha}$, where $\alpha < 1$. For very strong interaction between pomerons, $\alpha \to 2/3$. This limit leads to universal particle densities in the pp-, pA-, and AB-collisions. Due to a rather weak interaction between pomerons, even at LHC energies, the value of α is close to 0.9.

The problem of shadowing for inclusive spectra is not especially related to soft processes. The same interactions are also relevant for hard processes (production of jets or particles with large p_{T}, heavy quarks, large-mass lepton pairs, etc.). For hard processes, due to the QCD factorization theorem, inclusive spectra in nucleus–nucleus collisions are given by products of parton cross sections with distributions of partons in the nuclei. In these cases, interactions between pomerons describe shadowing effects for parton distributions in nuclei (or the nuclear structure functions described above). Due to the coherence condition, these effects are important only in the region of very small x_i of partons ($x_i \ll 1/(R_A m_N)$). Therefore, these effects are important only at very high energies, when $x_i \approx M_{\mathrm{T}}/\sqrt{s}$ satisfies this condition. The condition in terms of the x_i of partons coincides with the condition on diffractive production of large-mass states discussed above.

The effects of shadowing for soft partons were calculated in Ref. [76] in the same model that was used above for the description of shadowing effects for nuclear structure functions. It was predicted that extra shadowing due to interactions between pomerons leads to a decrease in particle densities compared to the GS model predictions by a factor ≈ 4 at LHC and by a factor ≈ 2 at RHIC energies. Comparison of the theoretic results with the first results from RHIC [77] is given in Table 2. The experiment clearly shows a large deviation from the prediction of the GS approximation and demonstrates the importance of the shadowing effects for inclusive spectra of hadrons. This approach also reproduces the dependence of particle densities at RHIC on the number of participating nucleons [78].

Table 2. Densities of charged hadrons $\mathrm{d}n/\mathrm{d}\eta|_{\eta=0}$ in central Pb–Pb collisions at $\sqrt{s} = 130$ GeV.

Glauber	With shadowing corrections	Experiment [77]
1200 ± 100	630 ± 120	$555 \pm 12 \pm 35$

These results show that already starting from the RHIC energies, interactions between pomerons (or strings) play an important role in the dynamics of heavy-ion collisions. On the other hand, characteristic partonic values $x_i \sim 10^{-2}$ at these energies and both experimental data on shadowing for nuclear structure functions [73] and their theoretical interpretation [72] show that the situation is very far from 'saturation' in this region.

7. Conclusion

The results presented in this review demonstrate that the Reggeon theory is a useful and universal approach for investigation of interactions of hadrons and nuclei at high energies. The pomeron is the main object in this approach.

The challenging problem for high-energy hadronic physics is to establish the dynamical nature of the pomeron. The analysis of this problem in QCD with inclusion of both nonperturbative and perturbative effects shows that the pomeron has a very rich dynamical structure.

The connection between the Reggeon theory, $1/N$-expansion in QCD, and string model leads to many relations between parameters of this theory and allows understanding many characteristic features of strong interactions. The quark–gluon strings and DPM models developed in the framework of this approach give a good description of many characteristics of high-energy hadronic interactions and give predictions for energies of future accelerators.

Multipomeron exchanges are very important at high energies. With the account of the unitarization effects for the amplitudes related to such exchanges, it is possible to understand and quantitatively describe small-x deep inelastic scattering. Interactions between pomerons are essential in hadron–nucleus and especially in nucleus–nucleus collisions, where the approach to thermalization and conditions for the quark–gluon plasma formation depend on the strength of interactions between strings. A reduction of the density of created hadrons due to these interactions compared to predictions of the GS model is confirmed by the RHIC data.

Acknowledgements. I would like to thank K Boreskov, A Capella, V Fadin, E G Ferreiro, O V Kancheli, V A Khoze, J H Koch, G Korchemski, E Levin, L N Lipatov, A Martin, C Merino, R A Salgado, K A Ter-Martirosyan, and J Tran Thanh Van for useful discussions.

This work was supported in part by the grants INTAS 00-00366, NATO PSTCLG- 997275, RFBR 00-19-25786, 01-02-17383

References

1. Feinberg E L, Pomeranchuk I Ya *Doklady Akad. Nauk SSSR* **94** 439 (1953); *Nuovo Cimento Suppl.* III 652 (1956)

2. Pomeranchuk I Ya *Zh. Eksp. Teor. Fiz.* **34** 725 (1958) [*Sov. Phys. JETP* **7** 499 (1958)]
3. Gribov V N, Pomeranchuk I Ya *Phys. Rev. Lett.* **8** 343, 312 (1962); *Nucl. Phys.* **38** 516 (1962); *Phys. Rev. Lett.* **9** 239 (1962)
4. Frautschi S C, Gell-Mann M, Zacharisen F *Phys. Rev.* **126** 2204 (1962)
5. 't Hooft G *Nucl. Phys. B* **72** 461 (1974)
6. Veneziano G *Phys. Lett. B* **52** 220 (1974)
7. Veneziano G *Nucl. Phys. B* **117** 519 (1976)
8. Ciafaloni M, Marchesini G, Veneziano G *Nucl. Phys. B* **98** 472 (1975)
9. Casher A, Kogut J, Susskind L *Phys. Rev. D* **10** 732 (1974)
10. Artru X, Mennesier G *Nucl. Phys. B* **70** 93 (1974)
11. Casher A , Neuberger H , Nussinov S *Phys. Rev. D* **20** 179 (1979)
12. Andersson B, Gustafson G, Peterson C *Phys. Lett. B* **71** 337 (1977); *Z. Phys. C: Part. Fields* **1** 105 (1979)
13. Gurvich E G *Phys. Lett. B* **87** 386 (1979)
14. Kaidalov A B *Pis'ma Zh. Eksp. Teor. Fiz.* **32** 494 (1980) [*JETP Lett.* **32** 474 (1980)]; *Yad. Fiz.* **33** 1369 (1981) [*Sov. J. Nucl. Phys.* **33** 733 (1981)]; *Phys. Lett. B* **116** 459 (1982); Kaidalov A B, Ter-Martirosyan K A *Phys. Lett. B* **117** 247 (1982); *Yad. Fiz.* **39** 1545; **40** 211 (1984) [*Sov. J. Nucl. Phys.* **39** 979; **40** 135 (1984)]
15. Kaidalov A B, in *QCD at 200 TeV* (Eds L Cifarelli, Yu Dokshitzer) (New York: Plenum Press, 1992) p. 1; *Surv. High Energy Phys.* **13** 265 (1999)
16. Capella A et al. *Z. Phys. C: Part. Fields* **3** 329 (1980); Capella A, Tran Thanh Van J *Phys. Lett. B* **114** 450 (1982); *Z. Phys. C: Part. Fields* **10** 249 (1981)
17. Capella A et al. *Phys. Rep.* **236** 225 (1994)
18. Regge T *Nuovo Cimento* **14** 951 (1959)
19. Gribov V N *Zh. Eksp. Teor. Fiz.* **41** 667 (1961) [*Sov. Phys. JETP* **14** 478 (1962)]
20. Chew G F, Frautschi S C *Phys. Rev. Lett.* **7** 394 (1961); Blankenbecler R, Goldberger M L *Phys. Rev.* **126** 766 (1962)
21. Froissart M *Phys. Rev.* **123** 1053 (1961)
22. Mandelstam S *Nuovo Cimento* **30** 1148 (1963)
23. Gribov V N, Pomeranchuk I Ya, Ter-Martirosyan K A *Phys. Lett.* **9** 269 (1964); *Yad. Fiz.* **2** 361 (1965) [*Sov. J. Nucl. Phys.* **2** 258 (1965)]
24. Amati D, Stanghellini A, Fubini S *Nuovo Cimento* **26** 896 (1962)
25. Chernavsky D S et al. *Nucl. Phys.* **44** 116 (1963); Akimov V N et al. *Nucl. Phys. B* **14** 285 (1969)
26. Dubin A, Kaidalov A, Simonov Yu *Phys. Lett. B* **323** 41 (1994); *Yad. Fiz.* **56** (12) 213 (1993) [*Phys. At. Nucl.* **56** 1745 (1993)]
27. Simonov Yu A *Nucl. Phys. B* **307** 512 (1988); *Yad. Fiz.* **54** 192 (1991) [*Sov. J. Nucl. Phys.* **54** 133 (1991)]
28. Simonov Yu A, hep-ph/0210309
29. Kuraev K A, Lipatov L N, Fadin V S *Zh. Eksp. Teor. Fiz.* **71** 840 (1976); **72** 377 (1977) [*Sov. Phys. JETP* **44** 443 (1976); **45** 199 (1977)]; Balitskii Ya Ya, Lipatov L N *Yad. Fiz.* **28** 1597 (1978) [*Sov. J. Nucl. Phys.* **28** 822 (1978)]
30. Fadin V S, Lipatov L N *Phys. Lett. B* **429** 127 (1998)
31. Brodsky S J et al. *Pis'ma Zh. Eksp. Teor. Fiz.* **70** 161 (1999) [*JETP* **70** 155 (1999)]
32. Simonov Yu A *Phys. Lett. B* **249** 514 (1990)
33. Kaidalov A B, Simonov Yu A *Phys. Lett. B* **477** 163 (2000); *Yad. Fiz.* **63** 1507 (2000) [*Phys. At. Nucl.* **63** 1428 (2000)]
34. Morningstar C, Peardon M *Phys. Rev. D* **60** 034509 (1999)
35. Teper M, hep-th/9812187
36. Gribov V N *Zh. Eksp. Teor. Fiz.* **53** 654 (1967) [*Sov. Phys. JETP* **26** 414 (1968)]
37. Kaidalov A B *Yad. Fiz.* **45** 1452 (1987) [*Sov. J. Nucl. Phys.* **45** 902 (1987)]
38. Abramovskii V A, Kancheli O V, Gribov V N *Yad. Fiz.* **18** 595 (1973) [*Sov. J. Nucl. Phys.* **18** 308 (1974)]
39. Ter-Martirosyan K A *Phys. Lett. B* **44** 377 (1973)
40. Kaidalov A B, Ter-Martirosyan K A, Shabel'skii Yu M *Yad. Fiz.* **43** 1282 (1986) [*Sov. J. Nucl. Phys.* **43** 822 (1986)]
41. Ter-Martirosyan K A *Yad. Fiz.* **44** 1260 (1986) [*Sov. J. Nucl. Phys.* **44** 817 (1986)]
42. Kaidalov A B, Ponomarev L A, Ter-Martirosyan K A *Yad. Fiz.* **44** 722 (1986) [*Sov. J. Nucl. Phys.* **44** 468 (1986)]
43. Kaidalov A B, Piskunova O I *Yad. Fiz.* **41** 1278 (1985) [*Sov. J. Nucl. Phys.* **41** 816 (1985)]; *Z. Phys. C: Part. Fields* **30** 145 (1985)
44. Kaidalov A B, Piskunova O I *Yad. Fiz.* **43** 1545 (1986) [*Sov. J. Nucl. Phys.* **43** 994 (1986)]
45. Piskunova O I *Yad. Fiz.* **56** (8) 176 (1993) [*Phys. At. Nucl.* **56** 1094 (1993)]
46. Arakelyan G N *Yad. Fiz.* **61** 1682 (1998) [*Phys. At. Nucl.* **61** 1570 (1998)]
47. Amelin N S et al. *Yad. Fiz.* **51** 512; **52** 272 (1990) [*Sov. J. Nucl. Phys.* **51** 327; **52** 172 (1990)]
48. Kaidalov A B et al. *Phys. Lett. B* **45** 493 (1973)
49. Kaidalov A B *Phys. Rep.* **50** 157 (1979)
50. Kang K, Nicolescu B *Phys. Rev. D* **11** 2461 (1975); Joynson D et al. *Nuovo Cimento A* **30** 345 (1975)
51. Lipatov L N *Phys. Lett. B* **309** 394 (1993); Gauron P, Lipatov L N, Nicolescu B *Phys. Lett. B* **304** 334 (1993); Faddeev L D, Korchemsky G P *Phys. Lett. B* **342** 311 (1995); Janik R A, Wosiek J *Phys. Rev. Lett.* **82** 1092 (1999)
52. Adloff C et al. (H1 Collab.) *Phys. Lett. B* **544** 35 (2002)
53. Ahmed T et al. (H1 Collab.) *Phys. Lett. B* **299** 374 (1993); Adloff C et al. (H1 Collab.) *Nucl. Phys. B* **497** 3 (1997)
54. Derrick M et al. (ZEUS Collab.) *Phys. Lett. B* **293** 465 (1992); Breitweg J et al. (ZEUS Collab.) *Phys. Lett. B* **407** 432 (1997)
55. Derrick M et al. (ZEUS Collab.) *Z. Phys. C: Part. Fields* **72** 399 (1996)
56. Adloff C et al. (H1 Collab.) *Z. Phys. C: Part. Fields* **76** 613 (1997)
57. Gribov L V, Levin E M, Ryskin M G *Phys. Rep.* **100** 1 (1983); Laenen E, Levin E *Annu. Rev. Nucl. Part.* **44** 199 (1994); Mueller A H, hep-ph/9911289
58. Mueller A H *Nucl. Phys. B* **437** 107 (1995); Gotsman E, Levin E, Maor U *Nucl. Phys. B* **493** 354 (1997); *Phys. Lett. B* **425** 369 (1998); **452** 387 (1999); McDermott M et al. *Eur. Phys. J. C* **16** 641 (2000); Golec-Biernat K, Wüsthoff M *Phys. Rev. D* **59** 014017; **60** 114023 (1999)
59. McLerran L, Venugopalan R *Phys. Rev. D* **49** 2233; **50** 2225 (1994); **53** 458 (1996); Jalilian-Marian J et al. *Phys. Rev.* **59** 014014, 034007 (1999); Kovner A, McLerran L, Weigert H *Phys. Rev. D* **52** 3809, 6231 (1995); Kovchegov Yu V, Mueller A H *Nucl. Phys. B* **529** 451 (1998); Mueller A H *Nucl. Phys. B* **558** 285 (1999)
60. Capella A et al. *Phys. Lett. B* **337** 358 (1994)
61. Kaidalov A B, Merino C *Eur. Phys. J. C* **10** 153 (1999)
62. Kaidalov A B, Merino C, Pertermann D *Eur. Phys. J. C* **20** 301 (2001)
63. Capella A et al. *Nucl. Phys. B* **593** 336 (2001); *Phys. Rev. D* **63** 054010 (2001)
64. Ioffe B L *Phys. Lett. B* **30** 123 (1969)
65. Bjorken J D, Kogut J B *Phys. Rev. D* **8** 1341 (1973)
66. Frankfurt L L, Strikman M *Phys. Rep.* **160** 235 (1988)
67. Nikolaev N N, Zakharov B G *Z. Phys. C: Part. Fields* **49** 607 (1990)
68. Capella A et al. *Phys. Lett. B* **343** 403 (1995); *Phys. Rev. D* **53** 2309 (1996)
69. Glauber R J, in *Lectures in Theoretical Physics* Vol. 1 (Ed. W E Britten) (New York: Interscience Publ., 1959) p. 315; Sitenko A G *Ukr. Fiz. Zh.* **4** 152 (1959)
70. Gribov V N *Zh. Eksp. Teor. Fiz.* **56** 892; **57** 1306 (1969) [*Sov. Phys. JETP* **29** 483; **30** 709 (1969)]
71. Schwimmer A *Nucl. Phys. B* **94** 445 (1975)
72. Capella A et al. *Eur. Phys. J. C* **5** 111 (1998)
73. Arneodo M et al. (NMC Collab.) *Nuovo Cimento A* **107** 2141 (1994); Amaudruz P et al. (NMC Collab.) *Nucl. Phys. B* **441** 3 (1995)
74. Kaidalov A B *Nucl. Phys. A* **525** 39 (1991)
75. Werner K *Phys. Rep.* **232** 87 (1993)
76. Capella A, Kaidalov A, Tran Thanh Van J *Heavy Ion Phys.* **9** 169 (1999)
77. Back B B et al. (PHOBOS Collab.) *Phys. Rev. Lett.* **87** 102303 (2001)
78. Capella A, Sousa D *Phys. Lett. B* **511** 185 (2001)